LIGHT AND EXOTIC MESONS

Curtis A. Meyer

Carnegie Mellon University, Pittsburgh, PA 15213

Abstract

1 Introduction

In this series of lectures I want to provide an overview of the field of *light–quark meson spectroscopy*. What do we understand about mesons? What does studying mesons tell us about QCD? How do we study mesons? Why do we study meson; what is exciting about this? The area of light–quark meson spectroscopy deals with mesons built up from u, d and s quarks. Typically, these systems have masses below $2.5\,\mathrm{GeV/c^2}$.

2 Mesons in the Quark Model

To do this, I want to start with the very basics of the strong interaction, namely the conserved quantities, **J**, **P**, **C**, $\cdots$. With this, I want to look at spectroscopy within one specific model, the *constituent quark model*. This model is by no means perfect. It provides no explanation for confinement, and the role of gluons is not obvious. It also makes no absolute mass predictions, and no absolute rate predictions for decays. However it does make a rather large number of very good predictions. It also provides a very natural framework within which to classify mesons. It provides a natural handle to address issues such as structure and decays, and even makes some rather nice predictions for relative decay rates.

The strong interaction conserves a number of quantities, some of which are listed here.

B Baryon number.

Q Electric charge.

J Angular momentum.

S Strangeness.

I Strong isospin.

P Parity.

C Charge conjugation.

G G–parity.

Those that are used will be explained as we go along. However, a number of these are carried by the quarks themselves. In table 1 are given the quantum numbers of the three lightest quarks.

Quark	**B**	**Q**	**J**	**S**	**I**	$\mathbf{I_z}$
u	$\frac{1}{3}$	$\frac{2}{3}$	$\frac{1}{2}$	0	$\frac{1}{2}$	$+\frac{1}{2}$
d	$\frac{1}{3}$	$-\frac{1}{3}$	$\frac{1}{2}$	0	$\frac{1}{2}$	$-\frac{1}{2}$
s	$\frac{1}{3}$	$-\frac{1}{3}$	$\frac{1}{2}$	-1	0	0

Table 1: Quantum numbers of the quarks. **B** is baryon number, **Q** is electric charge, **J** is the spin, **S** is strangeness, **I** is the strong isospin and $\mathbf{I_z}$ is the projection of **I** along the quantization axis, (usually defined as z).

In the constituent quark model, we treat a meson as a bound *quark-antiquark* pair, $q\bar{q}$, and then draw an analogy to the positronium system, e^+e^- to understand what we are seeing. In this picture the q and the $\bar{q}$ both have spin $\frac{1}{2}$. These can combine to either total spin $\mathbf{S} = 0$, or total spin $\mathbf{S} = 1$.

$$\mathbf{S} = 0 \ \frac{1}{\sqrt{2}}(\uparrow_1\downarrow_2 - \downarrow_1\uparrow_2) \quad \mathbf{S} = 1 \ \frac{1}{\sqrt{2}}(\uparrow_1\downarrow_2 + \downarrow_1\uparrow_2) \begin{matrix} \uparrow_1\uparrow_1 \\ \\ \downarrow_1\downarrow_2 \end{matrix}$$

In addition to the total spin, we can have orbital angular momentum **L** between the $q\bar{q}$ pair. Then, the **L** and **S** can combine to total angular momentum $\mathbf{J} = \mathbf{L} \oplus \mathbf{S}$, where $\mathbf{J} = \mid \mathbf{L} - \mathbf{S} \mid, \mid \mathbf{L} - \mathbf{S} + 1 \mid, \cdots, \mid \mathbf{L} + \mathbf{S} \mid$. The states can be written in spectroscopic notation as $^{\mathbf{2S+1}}\mathbf{L_J}$, and are shown for positronium in table 2. Using the quarks as given in table 1, we are then able to use **L**, **S** and **J** to construct the $\mathbf{J^{PC}}$ quantum numbers of the mesons. Let us start with parity, **P**. Mathematically,

State	S	L	J	P	C	J^{PC}	*Mesons*				*Name*
$^1S_0$	0	0	0	$-$	$+$	0^{-+}	π	η	η'	K	pseudoscalar
$^3S_1$	1	0	0	$-$	$-$	1^{--}	ρ	ω	ϕ	K^*	vector
$^1P_1$	0	1	1	$+$	$-$	1^{+-}	b_1	h_1	h_1'	K_1	pseudo–vector
$^3P_0$	1	1	0	$+$	$+$	0^{++}	a_0	f_0	f_0'	K_0^*	scalar
$^3P_1$	1	1	1	$+$	$+$	1^{++}	a_1	f_1	f_1'	K_1	axial vector
$^3P_2$	1	1	2	$+$	$+$	2^{++}	a_2	f_2	f_2'	K_2^*	tensor

Table 2: The positronium states as a function of **L**, **S** and **J**. These then correspond to the named mesons of the specified $\mathbf{J^{PC}}$.

parity is a reflection operator, and if the wave functions are eigenstates of the parity operator, then

$$\mathbf{P}(\psi(\vec{r})) = \psi(-\vec{r}) = \eta_P \psi(\vec{r}).$$

Since applying parity twice should return us to the original state, the eigenvalues of parity, η_P can only be ± 1. We can normally separate ψ into a radial and an angular piece,

$$\psi(\vec{r}) = \mathbf{R}(r) Y_{lm}(\theta, \phi).$$

In this case, the operation of parity leaves $\mathbf{R}$ unchanged, but transforms the angular piece to $Y_{lm}(\pi - \theta, \phi + \pi)$, and it can be shown that:

$$Y_{lm}(\pi - \theta, \phi + \pi) = (-1)^l Y_{lm}(\theta, \phi).$$

Finally, fermions and antifermions have intrinsic opposite parity. This leads to the parity of a meson being:

$$\mathbf{P}(q\bar{q}) = (-1)^{\mathbf{L}+1} \tag{1}$$

In considering that parity is conserved in a reaction, we consider the decay $A \rightarrow B + C$, where there is orbital angular momentum l between B and C. Parity conservation says that

$$\mathbf{P}(A) = \mathbf{P}(B) \cdot \mathbf{P}(C) \cdot (-1)^l. \tag{2}$$

The next quantum number is charge conjugation, $\mathbf{C}$, which represents a transformation of the particle into its antiparticle. This reverses several properties of the particle such as charge and magnetic moment. Clearly, in order for a particle to be an eigenstate of the $\mathbf{C}$ operator, it must be electrically neutral. If we consider the π°, then:

$$\mathbf{C} \mid \pi^\circ >= \eta_C \mid \pi^\circ >$$

where $\eta_C = \pm 1$. If we imagine a meson built from a quark and its antiquark, say $u\bar{u}$, with some total wave function of both its position and spin, Ψ.

$$\Psi(\vec{r}, \vec{s}) = \mathbf{R}(r) Y_{lm}(\theta, \phi) \chi(\vec{s})$$

The charge conjugation operator acting on this state reverses the meaning of u and $\bar{u}$. This has the effect of mapping $\vec{r}$ which points to the quark into $-\vec{r}$ so that it continues to point at the quark. Under the same arguments that we used in parity, this leads to a factor $(-1)^{\mathbf{L}+1}$. This also flips the spin wave functions, leading to a factor of (-1) for the $\mathbf{S} = 0$ case and a factor of $) + 1)$ for the $\mathbf{S} = 1$ case. This is a factor of $(-1)^{\mathbf{S}+1}$, which when combined with the $\mathbf{L}$ factor leads to:

$$\mathbf{C}(q\bar{q}) = (-1)^{\mathbf{L}+\mathbf{S}} \tag{3}$$

Clearly charged particles cannot be eigenstates of $\mathbf{C}$, $\mathbf{C} \mid \pi^+ >= \eta \mid \pi^- >$. However, if we were to apply the $\mathbf{C}$ operator followed by a rotation in isospin, $R = \exp(i\pi I_2)$ such that $\mid I, I_z > \rightarrow \mid I, -I_z >$, then charged particles could be eigenstates of this operator. We define the $\mathbf{G}$ parity operator as $\mathbf{G} = \mathbf{CR}$, and from this it is

easy to show that for a $q\bar{q}$ system, $\mathbf{G} = \mathbf{C} \cdot (-1)^{\mathbf{I}}$. These then lead to the following formulas.

$$\mathbf{J} = \mathbf{L} \oplus \mathbf{S} \tag{4}$$
$$\mathbf{P} = (-1)^{\mathbf{L}+1} \tag{5}$$
$$\mathbf{C} = (-1)^{\mathbf{L}+\mathbf{S}} \tag{6}$$
$$\mathbf{G} = (-1)^{\mathbf{L}+\mathbf{S}+\mathbf{I}} \tag{7}$$

Using these relationships to build up possible $\mathbf{J^{PC}}$'s for mesons, we find that the following numbers are allowed:

$$0^{-+}, 0^{++}, 1^{--}, 1^{+-}, 1^{--}, 2^{--}, 2^{-+}, 2^{++}, 3^{--}, 3^{+-}, 3^{--}, \cdots$$

and looking carefully at these, we find that there is a sequence of $\mathbf{J^{PC}}$'s which are not allowed for a simple $q\bar{q}$ system.

$$0^{--}, 0^{+-}, 1^{-+}, 2^{+-}, 3^{-+}, \cdots$$

These latter quantum numbers are known as *explicitly exotic* quantum numbers. If a state with these quantum numbers is found, we know that it must be something other than a normal, $q\bar{q}$ meson.

Following the positronium analogy as in table 2, we can now assign the $\mathbf{J^{P(C)}}$ quantum numbers to the listed atomic states. In the case of mesons, we have three quarks, u, d and s which can be combined with three antiquarks. This leads to nine possible $q\bar{q}$ combinations with the same $\mathbf{J^{P(C)}}$, rather than the one positronium state. If we now assume that the three quarks are flavor symmetric, then we can use the SU(3)–flavor group to build up the nominal nine mesons, (a nonet).

$$\mathbf{3} \otimes \overline{\mathbf{3}} = \mathbf{1} \oplus \mathbf{8}$$

The nine members of the nonet are going to be broken into two groups, eight members of an octet, $\mid \mathbf{8} >$ and a single member of a singlet $\mid \mathbf{1} >$. Under the SU(3) flavor assumption, all the members of the octet have the same basic coupling constants to similar reactions, while the singlet member could have a different coupling. The nominal $q\bar{q}$ combinations for the pseudoscalar mesons are shown below. The three π's are isospin $I = 1$, while the K's are all isospin $\frac{1}{2}$. The $\mid 1 >$ and $\mid 8 >$ state are isospin 0.

$$\begin{array}{ccccc} & K^\circ & & K^+ & \\ \pi^- & & \pi^\circ, \eta, \eta' & & \pi^+ \\ & \bar{K}^\circ & & K^- & \end{array}$$

$$\begin{array}{ccccc} & (d\bar{s}) & & (u\bar{s}) & \\ (d\bar{u}) & & \frac{1}{\sqrt{2}}(u\bar{u} - d\bar{d}) & & (u\bar{d}) \\ & (s\bar{d}) & & (s\bar{u}) & \end{array} \tag{8}$$

$$\mid 8 > = \frac{1}{\sqrt{6}}(u\bar{u} + d\bar{d} - 2s\bar{s}) \quad \mid 1 > = \frac{1}{\sqrt{3}}(u\bar{u} + d\bar{d} + s\bar{s}) \tag{9}$$

There is also a well prescribed naming scheme for the mesons as given in [caso98] which is summarized in table 3. This of course leads to an entire zoo of particles, but the name itself gives you all the quantum numbers of the state. If we put all of this together, we obtain an entire expected spectrum of mesons as shown in Fig. 1. Where no state is indicated, the meson has not been observed, while the dark names indicate well established states.

$q\bar{q}$	Isospin	${}^1(L_{\rm even})_J$	${}^1(L_{\rm odd})_J$	${}^3(L_{\rm even})_J$	${}^3(L_{\rm odd})_J$
$u\bar{d}$,$u\bar{u}-d\bar{d}$,$d\bar{u}$	$I=1$	π_J	b_J	ρ_J	a_J
$s\bar{s}$,$u\bar{u}+d\bar{d}$	$I=0$	η_J,η'_J	h_J,h'_J	ω_J,ϕ_J	f_J,f'_J
$u\bar{s}$,$d\bar{s}$	$I=\frac{1}{2}$	$J^P=0^-,1^+,2^-,\cdots$	K_J	$J^P=0^+,1^-,2^+,\cdots$	K_J^*

Table 3: Naming Scheme of the light–quark mesons.

Because the SU(3) flavor symmetry is not exact, the $\mid 8 >$ and $\mid 1 >$ states discussed above, (equation 9), are not necessarily the physical states. The two isospin zero states can mix to form the observed states. There is a bit of historical confusion about how the mixing should be written - enough so that it is worth discussing it. In an older reference, (*e.g* [close79]), the nonet mixing is written in terms of a mixing angle, ϑ, as follows in equation 10.

$$\begin{pmatrix} f \\ f' \end{pmatrix} = \begin{pmatrix} \cos\vartheta & \sin\vartheta \\ -\sin\vartheta & \cos\vartheta \end{pmatrix} \begin{pmatrix} \mid 8> \\ \mid 1> \end{pmatrix} \tag{10}$$

In this parametrization, the so-called ideal mixing is given for $\cos\vartheta = \sqrt{\frac{1}{3}}$ and $\sin\vartheta = \sqrt{\frac{2}{3}}$, or $\vartheta = 54.74°$. For this particular angle, the mixed states can easily shown to be as in equation 11.

$$\begin{pmatrix} f \\ f' \end{pmatrix} = \begin{pmatrix} \frac{1}{\sqrt{2}}(u\bar{u}+d\bar{d}) \\ s\bar{s} \end{pmatrix} \tag{11}$$

If one looks in the *Particle Data Book* [caso98], then the mixing is parametrized using a nonet mixing angle θ_n as in equation 12.

$$\begin{pmatrix} f \\ f' \end{pmatrix} = \begin{pmatrix} \cos\theta_n & \sin\theta_n \\ -\sin\theta_n & \cos\theta_n \end{pmatrix} \begin{pmatrix} \mid 1> \\ \mid 8> \end{pmatrix} \tag{12}$$

In this scheme, the ideal mixing occurs for the choice of $\theta_n = 35.26°$, ($\cos\theta_n = \sqrt{\frac{2}{3}}$, $\sin\theta_n = \sqrt{\frac{1}{3}}$). Under this assumption, the physical states have the quark content as in equation 13. Most nonet mixing angles are now quoted in terms of this latter scheme, equation 12, and not in terms of equation 10.

$$\begin{pmatrix} f \\ -f' \end{pmatrix} = \begin{pmatrix} \frac{1}{\sqrt{2}}(u\bar{u}+d\bar{d}) \\ s\bar{s} \end{pmatrix} \tag{13}$$

It is possible to simply relate these two parameterizations, and can be easily shown that they are the same if $\vartheta = 90° - \theta_n$. Finally, to make matters even worse, the

pseudo-scalar mesons are often written in a different mixing scheme [genz83]. One way to understand this is to imagine that the η and the η' are interchanged, and that their names are the result of history. In any case, in terms of the pseudo-scalar mixing angle, θ_P, their mixing is given as in equation 14.

$$\begin{pmatrix} \eta' \\ \eta \end{pmatrix} = \begin{pmatrix} \cos\theta_P & \sin\theta_P \\ -\sin\theta_P & \cos\theta_P \end{pmatrix} \begin{pmatrix} \mid 1> \\ \mid 8> \end{pmatrix} \tag{14}$$

In the case of ideal mixing, $\theta_P = 35.26°$, it is the η which becomes an $s\bar{s}$ pair, and the η' which becomes purely a light quark system. Currently, the best value of the mixing angle is $\theta_P = -17°$. Using this angle, the η' is about 90% SU(3) singlet and the η is about 90% SU(3) octet. This can also be written in terms of the ideally mixed states as in equation 15, which shows the η' as 62% $s\bar{s}$.

$$\begin{pmatrix} \eta' \\ \eta \end{pmatrix} = \begin{pmatrix} 0.61 & 0.79 \\ 0.79 & -0.61 \end{pmatrix} \begin{pmatrix} \mid \frac{1}{\sqrt{2}}(u\bar{u} + d\bar{d}) > \\ \mid s\bar{s} > \end{pmatrix} \tag{15}$$

Finally, it is possible to use these SU(3) wave functions to predict mass relations between members of a meson nonet. For a pure nonet, one can derive a generalized linear mass formula, (equation 16). This formula is useful in predicting the masses of nonet members, and also verifying that a set of states can actually form a nonet.

$$(m_f + m_{f'})(4m_K - m_a) - 3m_f m_{f'} = 8m_K^2 - 8m_K m_a + 3m_a^2 \tag{16}$$

In addition to the linear mass formula, it is also possible to predict the nonet mixing angle, θ_n purely from the masses. Equation 17 can be used to determine the mixing angles, and when applied to three well established nonets, we find the mixing angles given in table 4. What is particularly interesting is that the three nonets are all reasonably close to ideally mixed. It appears that in many situation, nature wants to separate the light quarks, ($u\bar{u}$ and $d\bar{d}$) from the heavier s–quarks, ($s\bar{s}$). In fact, there are only two clear situation where this angle appears not to be ideally mixed. The ground state pseudoscalar mesons, where other effects are important, and the scalar mesons, where a glueball may be mixed into the nonet. If there are other nonets which are not ideally mixed is an open and important question.

$$\tan^2\theta_n = \frac{3m_{f'} - 4m_K + m_a}{4m_K - m_a - 3m_f} \tag{17}$$

$\mathbf{J^{PC}}$	a	f	f'	K	θ_n
1^{--}	$\rho(770)$	$\omega(782)$	$\phi(1020)$	$K^*(892)$	36.6°
2^{++}	$a_2(1320)$	$f_2(1270)$	$f_2'(1525)$	$K_2^*(1430)$	29.3°
3^{--}	$\rho_3(1690)$	$\omega_3(1670)$	$\phi_3(1850)$	$K_3^*(1780)$	31.0°

Table 4: Mixing Angles for well established nonets as computed using equation 17.

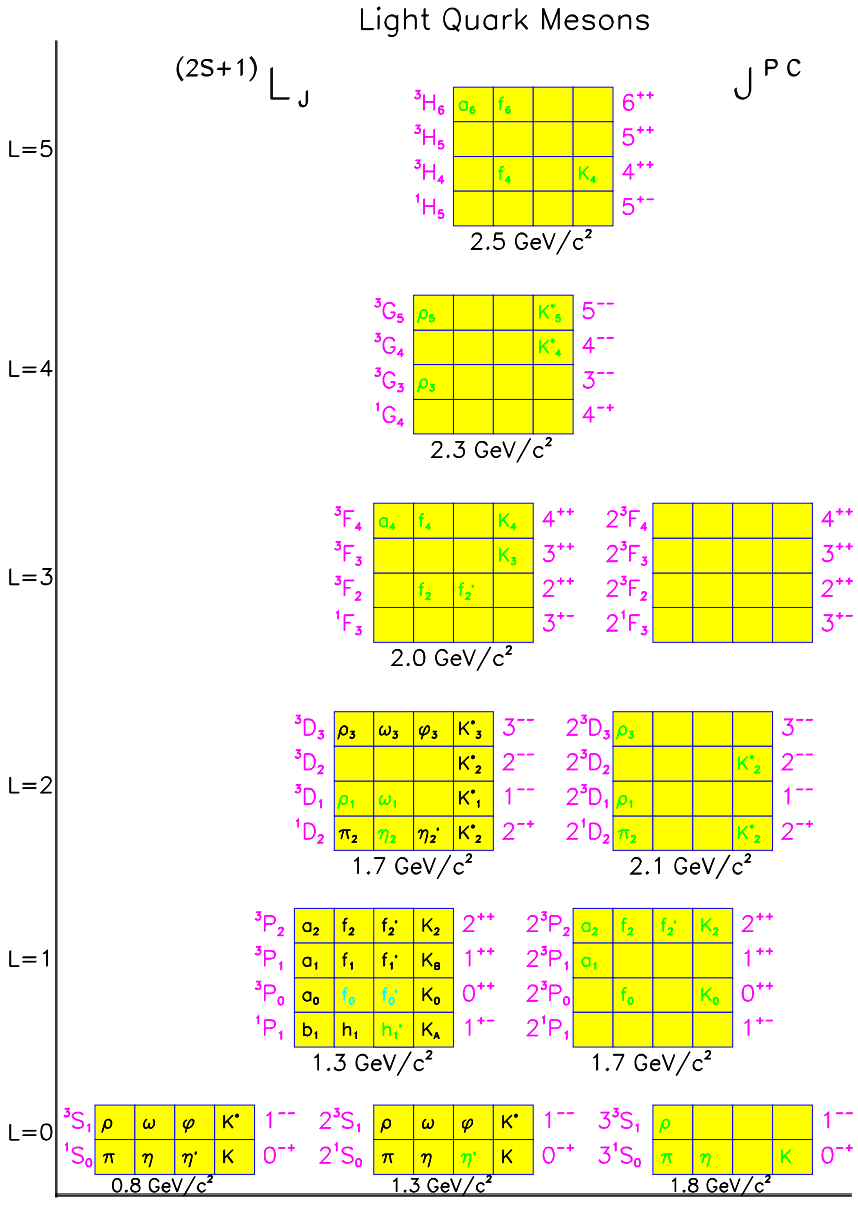

Figure 1: The expected meson spectrum showing the $^{2S+1}L_J$ representation, the J^{PC} of the nonet, and the names of the states. Along the vertical axis are plotted nonets for increasing values of **L**, while along the horizontal are plotted radial excitations. The average masses are indicated under the boxes. Dark names indicate well established states, while the lighter names are tentative assignments. All other states have not yet been observed.

3 Decays of Mesons

While the quark model does not make absolute decay predictions, we can use the conservation laws of the strong interaction to determine if a decay is possible. We can also use the SU(3) flavor symmetry to make predictions for relative strengths of decays.

We will first take up the use of conservation laws. Consider the decay $a_2^\circ \to \eta\pi^\circ$. The a_2 has $(\mathbf{I^G})\mathbf{J^{PC}} = (1^-)2^{++}$, the π has $(\mathbf{I^G})\mathbf{J^{PC}} = (1^-)0^{-+}$ and the η has $(\mathbf{I^G})\mathbf{J^{PC}} = (0^+)0^{-+}$.

$$a_2 \to \eta\pi \;\; (1^-)2^{++} \to \underbrace{(0^+)0^{-+} \oplus (1^-)0^{-+}}_{L_{\eta\pi}}$$

The only way for this reaction to conserve angular momentum, $\mathbf{J}$, is to have $L_{\eta\pi} = 2$. Under this assumption we can now check the remaining quantum numbers:

$\mathbf{P}$: $(+1) = (-1)(-1)(-1)^2 = (+1)$ — Parity is OK.

$\mathbf{C}$: $(+1) = (-1)(-1)$ — Charge conjugation is OK.

$\mathbf{G}$: $(\mathbf{-}1) = (+1)(\mathbf{-})1)$ — G–Parity is OK.

$\mathbf{I}$: $< I, I_z \mid I_1, I_2, I_{1z}, I_{2z} >=< 1, 0 \mid 1, 0, 0, 0 >= 1$ — Isospin is OK.

The reaction is not prevented by any conservation laws. We now look at a second reaction involving an f_1 decay to two π°'s. The f_1 has $(\mathbf{I^G})\mathbf{J^{PC}} = (0^+)1^{++}$, and both pions are $(1^-)0^{-+}$ states.

$$f_1 \to \pi^\circ\pi^\circ \;\; (0^+)1^{++} \to \underbrace{(1^-)0^{-+} \oplus (1^-)0^{-+}}_{L_{\pi\pi}}$$

The only way for this reaction to conserve angular momentum, $\mathbf{J}$, is to have $L_{\pi\pi} = 1$. Under this assumption we can now check the remaining quantum numbers:

$\mathbf{P}$: $(+1) = (-1)(-1)(-1)^1 = (-1)$ — Parity fails.

$\mathbf{C}$: $(+1) = (-1)(-1)$ — Charge conjugation is OK.

$\mathbf{G}$: $(+1) = (\mathbf{-}1)(\mathbf{-}1)$ — G–Parity is OK.

$\mathbf{I}$: $< I, I_z \mid I_1, I_2, I_{1z}, I_{2z} >=< 0, 0 \mid 1, 1, 0, 0 >= \frac{1}{\sqrt{3}}$ — Isospin is OK.

This reaction is prevented by parity conservation.

These exercises can tell us if a particular reaction is allowed. However they don't tell us anything about the rate of the reaction. In order to try and say more, we will invoke our SU(3) flavor symmetry. Under this symmetry, all members of a particular representation should have the same decay rates, modulo some sort of SU(3) Clebsch–Gordon coefficients.

$$\mathbf{8} \otimes \mathbf{8} = \mathbf{27} \oplus \mathbf{10} \oplus \mathbf{10} \oplus \mathbf{8} \oplus \mathbf{8} \oplus \mathbf{1}$$

In particular, there is one coupling constant for each type of allowed SU(3) transition.

$$\left.\begin{array}{ll} |\,8> \rightarrow |\,8> \otimes |\,8> & g_T \\ |\,8> \rightarrow |\,8> \otimes |\,1> & g_{18} \\ |\,1> \rightarrow |\,8> \otimes |\,8> & g_1 \\ |\,1> \rightarrow |\,1> \otimes |\,1> & g_{11} \end{array}\right\} \text{Allowed under SU(3)} \tag{18}$$

We will use the SU(3) flavor symmetry to compute decay amplitudes, γ. However, in order to compare to measured branching fractions, we need to turn these into decay rates, Γ as given in equation 19.

$$\Gamma = \gamma^2 \cdot f_L(q) \cdot q \tag{19}$$

If we consider the reaction $A \rightarrow BC$ as shown in Fig 2, then the quantity q is the momentum of B and C as seen in the rest frame of A.

$$q = \frac{\sqrt{(m_A^2 - (m_B + m_C)^2)(m_A^2 - (m_B - m_C)^2)}}{2m_A}$$

q is related to the available phase–space via $\rho = 2q/m$. In addition, there is an angular momentum barrier factor $f_L(q)$ which depends on the relative $\mathbf{L}$ between B and C, and their momentum q. For small q, we expect this to scale like q^{2L}. An empirical form for this factor is given as in equation 20 where $\beta \sim 0.4\,\text{to}\,0.5\,\text{GeV/c}$.

$$f_L(q) = q^{2L} \exp\left(-\frac{q^2}{8\beta^2}\right) \tag{20}$$

The form of $f_L(q)$ is shown in Fig. 2 for $L = 0, 1, 2$. A rule of thumb is that a decay needs about 200 MeV/c of momentum for each unit of $\mathbf{L}$. In order to use these, we need the SU(3) Clebsch–Gordon coefficients. The ones which are applicable to meson decays are given as follows.

$$\begin{array}{l} |\,1> \rightarrow |\,8> \otimes |\,8> \\ (\eta_1) \rightarrow \Big((K^+, K^\circ)\bar{K}\ (\pi^+, \pi^\circ, \pi^-)\pi^\circ\ \eta\eta\ (K^-, \bar{K}^\circ) \Big) \\ \qquad \frac{1}{\sqrt{8}} \begin{pmatrix} 2 & 3 & -1 & -2 \end{pmatrix}^{\frac{1}{2}} \end{array}$$

$$\begin{array}{l} |\,8> \rightarrow |\,8> \otimes |\,8> \\ \begin{pmatrix} K \\ \pi \\ \eta_8 \\ \bar{K} \end{pmatrix} \rightarrow \begin{pmatrix} K\pi & K\eta & \pi K & \eta K \\ K\bar{K}\ \pi\pi & \eta\pi & \pi\eta & \bar{K}K \\ K\bar{K}\ \pi\pi & \eta\eta & & \bar{K}K \\ \pi\bar{K} & \eta\bar{K} & \bar{K}\pi & \bar{K}\eta \end{pmatrix} \\ \qquad \frac{1}{\sqrt{(20}} \begin{pmatrix} 9 & -1 & -9 & -1 \\ -6 & 0 & 4 & 4 & -6 \\ 2 & -12 & -4 & & -2 \\ 9 & -1 & -9 & -1 \end{pmatrix} \end{array}$$

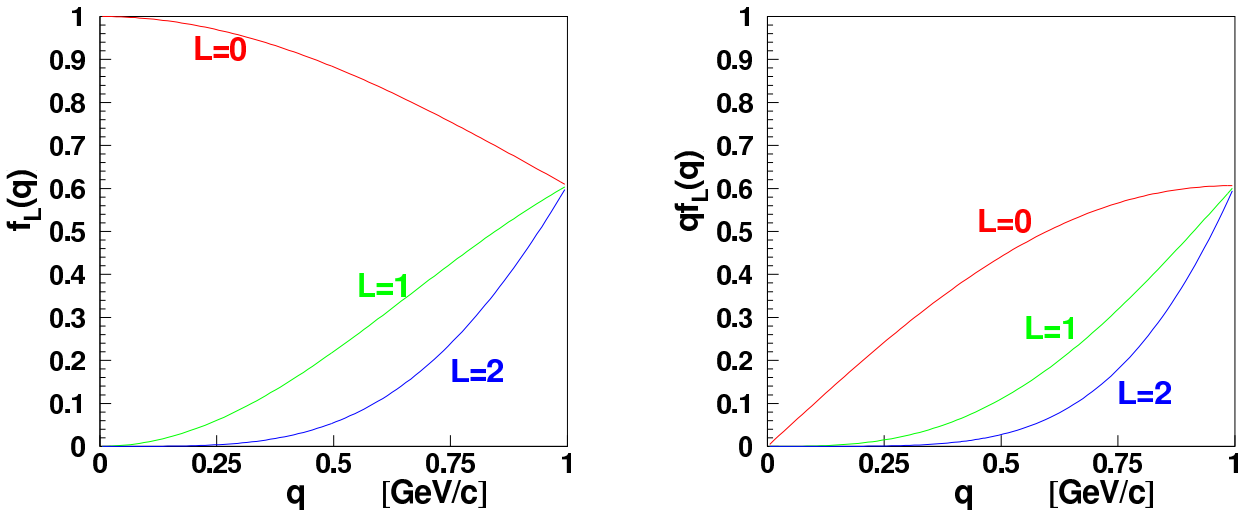

Figure 2: **a** The form factor, $f_L(q)$, for the Decay $A \to BC$ as a function of the q of the reaction. **b** The form factor multiplied by the momentum q for the same decay, $qf_L(q)$. The three curves are for different orbital angular momentum, L and the form factor is given in equation 20.

We can now use these coefficients in conjunction with the four decay constants to compute decay rates. As an example, let us consider the decay $f \to \pi\pi$. We will ignore the **J** of the f for the moment, and only assume that the reaction is allowed by our basic conservation laws, (this is true for **J** even). We also need to break the f into its octet, f_8, and singlet, f_1 pieces. Recall that in the PDG mixing scheme, $f = \sin\theta f_8 + \cos\theta f_1$ and $f' = \cos\theta f_8 - \sin\theta f_1$ and that ideal mixing occurs when $\cos\theta = \sqrt{\frac{2}{3}}$ and $\sin\theta = \sqrt{\frac{1}{3}}$. From this, we can write the amplitude for our decay as:

$$\begin{aligned}\gamma(f \to \pi\pi) &= \gamma\left([\sin\theta f_8 + \cos\theta f_1] \to \pi\pi\right) \\ &= \sin\theta \underbrace{\gamma(f_8 \to \pi\pi)}_{g_T \cdot -\sqrt{\frac{12}{20}}} + \cos\theta \underbrace{\gamma(f_1 \to \pi\pi)}_{g1 \cdot \sqrt{\frac{3}{8}}}\end{aligned}$$

$$\gamma(f \to \pi\pi) = -\sqrt{\frac{3}{5}} g_T \sin\theta + \sqrt{\frac{3}{8}} g_1 \cos\theta \tag{21}$$

Similarly, we can examine the decay $f \to K\bar{K}$. The only difference is the Clebsch–Gordon coefficients, which when putting it together yields equation 22.

$$\gamma(f \to K\bar{K}) = \sqrt{\frac{1}{10}} g_T \sin\theta + \frac{1}{2} g_1 \cos\theta \tag{22}$$

Similarly, we can examine the decays of f' by writing it in terms of f_1 and f_8 as in equation 12. For the $\pi\pi$ decay, this yields equation 23.

$$\gamma(f' \to \pi\pi) = -\sqrt{\frac{3}{5}} g_T \cos\theta - \sqrt{\frac{3}{8}} g_1 \sin\theta \tag{23}$$

If we had considered ideal mixing, (see equation 13), then we could compute the rate for $s\bar{s}$ into $\pi\pi$ as given in equation 24.

$$\gamma(s\bar{s} \to \pi\pi) = -\sqrt{\frac{3}{5}} g_T \sqrt{\frac{2}{3}} - \sqrt{\frac{3}{8}} g_1 \sqrt{\frac{1}{3}} \tag{24}$$

At this point we want to invoke something called the *Zweig rule*, or *OZI suppression*. This basically says that diagrams that destroy the initial quark and antiquark are strongly suppressed with respect to those that do not. In Fig. 3 are shown examples of these, where **a** shows the initial quarks destroyed and **b** shows them preserved. This observation comes from $c\bar{c}$ decays where the Ψ states below the open charm threshold have very narrow widths, but after the threshold for D production is crossed, the widths become much larger. Our reaction $s\bar{s} \to \pi\pi$ is an example of one of the suppressed diagrams, and we are going to set the rate for this to zero. Doing this, equation 24 gives us that $g_1 = -\frac{4}{\sqrt{5}} g_T$.

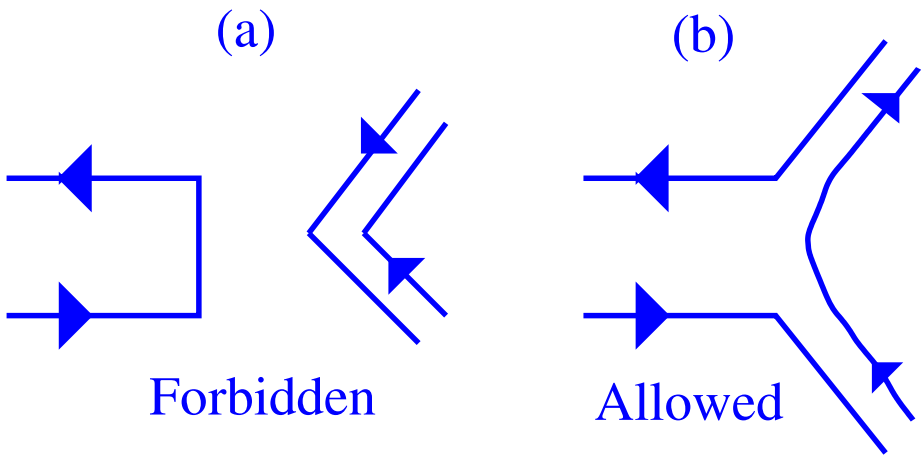

Figure 3: **a**) OZI forbidden and **b** OZI allowed decays.

Two other reactions, 25 and 26, should also be *OZI* suppressed and we will set their rates to be zero.

$$\left[u\bar{u}/d\bar{d}\right] \to [s\bar{s}]\,\pi \tag{25}$$

$$\left[u\bar{u}/d\bar{d}\right] \to [s\bar{s}]\,[s\bar{s}] \tag{26}$$

For reaction 25, an example of such a decay is $a \to [s\bar{s}]\,\pi$, where we find the decay rate as:

$$\gamma(a \to [s\bar{s}]\,\pi) = -\sqrt{\frac{2}{3}} \underbrace{\gamma(a_8 \to \eta_8\pi_8)}_{\sqrt{\frac{4}{20}} g_T} + \sqrt{\frac{1}{3}} \underbrace{\gamma(a_8 \to \eta_1\pi_8)}_{g_{18}}.$$

Setting this rate equal to 0 yields the relation: $g_{18} = \sqrt{\frac{2}{5}} g_T$. Doing the same thing for reaction 26, we can write that the isospin 0 light quark mixture is:

$$\frac{1}{\sqrt{2}}(u\bar{u} + d\bar{d}) = \sqrt{\frac{1}{3}} f_8 + \sqrt{\frac{2}{3}} f_1.$$

We then examine its decay amplitude to two $s\bar{s}$ pairs as follows.

$$\begin{aligned}
0 &= \gamma \left[\left(\sqrt{\frac{1}{3}} f_8 + \sqrt{\frac{2}{3}} f_1 \right) \rightarrow \left(\sqrt{\frac{2}{3}} \eta_8 - \sqrt{\frac{1}{3}} \eta_1 \right) \left(\sqrt{\frac{2}{3}} \eta_8 - \sqrt{\frac{1}{3}} \eta_1 \right) \right] \\
0 &= \sqrt{\frac{1}{3}} \left[\frac{2}{3} \gamma(f_8 \rightarrow \eta_8 \eta_8) + \frac{1}{3} \gamma(f_8 \rightarrow \eta_1 \eta_1) - \frac{2\sqrt{2}}{3} \gamma(f_8 \rightarrow \eta_1 \eta_8) \right] \\
&\quad + \sqrt{\frac{2}{3}} \left[\frac{2}{3} \gamma(f_1 \rightarrow \eta_8 \eta_8) + \frac{1}{3} \gamma(f_1 \rightarrow \eta_1 \eta_1) - \frac{2\sqrt{2}}{3} \gamma(f_1 \rightarrow \eta_1 \eta_8) \right] \\
0 &= \sqrt{\frac{1}{3}} \left[\frac{2}{3} (-\frac{1}{\sqrt{5}}) g_T - \frac{2\sqrt{2}}{3} g_{18} \right] + \sqrt{\frac{2}{3}} \left[\frac{2}{3} (-\frac{1}{\sqrt{8}}) g_1 + \frac{1}{3} g_{11} \right]
\end{aligned}$$

Decay	Constant	Constant/g_T
$\mid 8 > \rightarrow \mid 8 > \otimes \mid 8 >$	g_T	1.00
$\mid 8 > \rightarrow \mid 8 > \otimes \mid 1 >$	g_{18}	$\sqrt{\frac{2}{5}}$
$\mid 1 > \rightarrow \mid 8 > \otimes \mid 8 >$	g_1	$-\frac{4}{\sqrt{5}}$
$\mid 1 > \rightarrow \mid 1 > \otimes \mid 1 >$	g_{11}	$\sqrt{\frac{2}{5}}$

Table 5: The four SU(3) decay constants expressed in terms of the single constant g_T under the assumption of perfect OZI supression.

Which yields that $g_{11} = \sqrt{\frac{2}{5}} g_T$. We now have sufficient information to express all the decay amplitudes of a given nonet in terms of one unknown decay constant, g_T, (see table 5). These are given as a function of both the nonet mixing angle, θ and the pseudoscalar angle, θ_P. If we take $\theta_P = -17°$, then we can plot γ^2 as a function of θ; these are shown in Fig. 4.

$$\begin{aligned}
\gamma(f \rightarrow \pi\pi) &= -\sqrt{\frac{3}{5}} \left(\sin\theta + \sqrt{2}\cos\theta \right) g_T \\
\gamma(f' \rightarrow \pi\pi) &= -\sqrt{\frac{3}{5}} \left(\cos\theta - \sqrt{2}\sin\theta \right) g_T \\
\gamma(f \rightarrow K\bar{K}) &= \sqrt{\frac{1}{10}} \left(\sin\theta - 2\sqrt{2}\cos\theta \right) g_T \\
\gamma(f' \rightarrow K\bar{K}) &= \sqrt{\frac{1}{10}} \left(\cos\theta + 2\sqrt{2}\sin\theta \right) g_T
\end{aligned}$$

$$\gamma(f \to \eta\eta) = \sqrt{\frac{1}{5}} \left\{ \sqrt{2}\cos\theta - \sin\theta \left(\cos^2\theta_P + 2\sqrt{2}\cos\theta_P \sin\theta_P \right) \right\} g_T$$

$$\gamma(f' \to \eta\eta) = \sqrt{\frac{1}{5}} \left\{ \sqrt{2}\sin\theta + \cos\theta \left(\cos^2\theta_P + 2\sqrt{2}\cos\theta_P \sin\theta_P \right) \right\} g_T$$

$$\gamma(f \to \eta\eta') = \frac{1}{2\sqrt{5}} \sin\theta \left\{ 2\sqrt{2}\cos(2\theta_P) - \sin(2\theta_P) \right\} g_T$$

$$\gamma(f' \to \eta\eta') = \frac{1}{2\sqrt{5}} \cos\theta \left\{ 2\sqrt{2}\cos(2\theta_P) - \sin(2\theta_P) \right\} g_T$$

$$\gamma(f \to \eta'\eta') = \sqrt{\frac{1}{5}} \left\{ \sqrt{2}\cos\theta - \sin\theta \left(\sin^2\theta_P - 2\sqrt{2}\cos\theta_P \sin\theta_P \right) \right\} g_T$$

$$\gamma(f' \to \eta'\eta') = \sqrt{\frac{1}{5}} \left\{ \sqrt{2}\sin\theta + \cos\theta \left(\sin^2\theta_P - 2\sqrt{2}\cos\theta_P \sin\theta_P \right) \right\} g_T$$

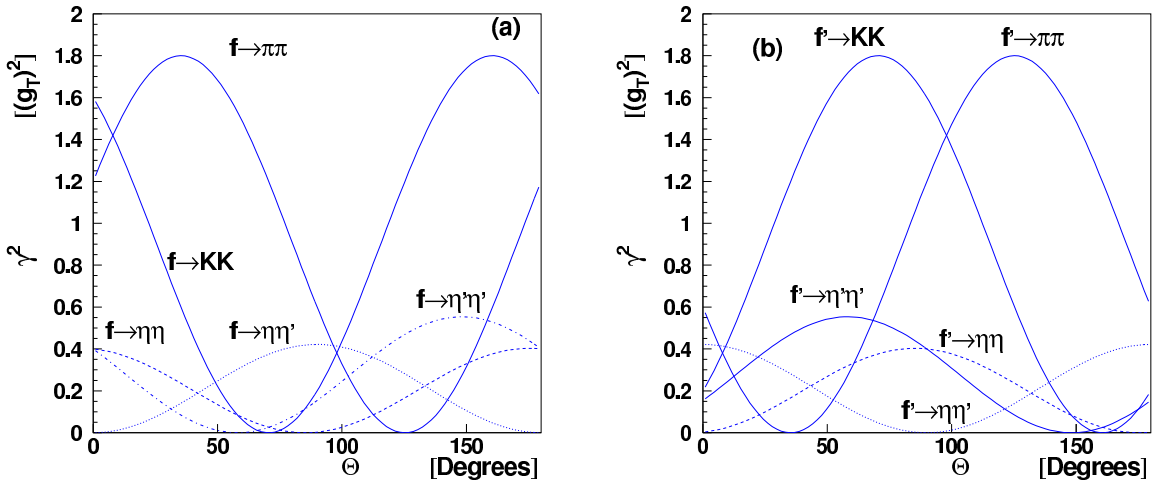

Figure 4: Decay amplitudes, γ^2, as a function of nonet mixing angle θ. (**a**) is for f decays while (**b**) is for f' decays. The pseudoscalar mixing angle is taken as $\theta_P = -17°$.

This simple prediction does a remarkably good job in describing the tensor mesons, $J^{PC} = 2^{++}$. From [caso98] we find the decay rates to two pseudoscalars as given in table 6. In addition, using the masses as given in table 4 and the mass formula from equation 17, we find an optimum mixing angle of $(29.3 \pm 1.6)°$. We can also use the decay information to fit for the mixing angle as well. In Figure 5 is shown the results of such a fit, where the optimum value comes out as 32.8°. This is in remarkably good agreement with the simple mass prediction.

State	Decay	Rate	q $[GeV/c]$	$qf_2(q)$	γ^2
$f_2(1270)$	$\rightarrow \pi\pi$	0.846 ± 0.02	0.622	0.118	11.54 ± 0.27
	$\rightarrow K\bar{K}$	0.046 ± 0.004	0.327	0.0236	4.84 ± 0.42
	$\rightarrow \eta\eta$	0.0045 ± 0.0015	0.402	0.0107	1.29 ± 0.43
$f_2'(1525)$	$\rightarrow \pi\pi$	0.0082 ± 0.0015	0.749	0.223	0.049 ± 0.009
	$\rightarrow K\bar{K}$	0.888 ± 0.031	0.580	0.0919	16.65 ± 0.58
	$\rightarrow \eta\eta$	0.103 ± 0.031	0.531	0.0668	2.90 ± 0.87
$a_2(1320)$	$\rightarrow \eta\pi$	0.145 ± 0.012	0.535	0.0686	3.95 ± 0.33
	$\rightarrow \eta'\pi$	0.0053 ± 0.0009	0.287	0.0064	2.86 ± 0.49
	$\rightarrow K\bar{K}$	0.049 ± 0.008	0.437	0.0324	3.46 ± 0.56

Table 6: Experimental decay rates for the tensor mesons decaying to pairs of pseudoscalar mesons. The factor γ^2 is the rate corrected for both phase space and barrier factors as in equation 19.

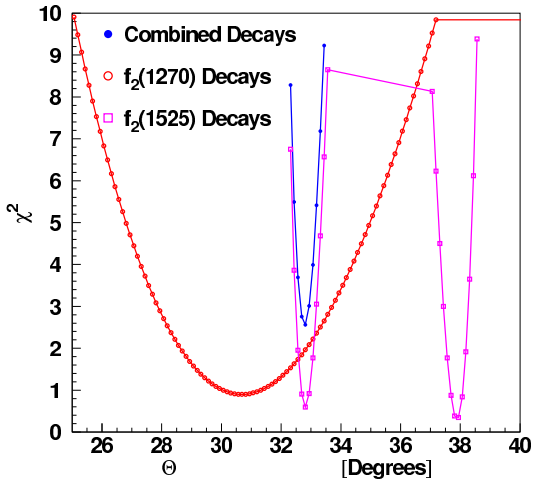

Figure 5: The χ^2 as a function of nonet mixing angle for the tensor mesons. The *combined decays* optimizes for a mixing angle of about 32.8°.

4 Exotic Mesons

If it were just for normal $q\bar{q}$ mesons, one could argue that there is not really a lot to do in light–quark meson spectroscopy. The *quark model* does a nice job of explaining things, and when extended to the *flux tube model*, with the $^3P_0$ model for decays, a very nice picture appears. In fact, a picture which is quite consistent with known meson phenomenology. To this, we can add *lattice QCD* calculations, and the picture improves. A good picture of masses and decays emerges which is reasonably consistent with data. So, why are we continuing to study this? What is there that we can still learn?

The *quark model* has no confinement and in fact we don't even need gluons in the picture. However, things like the *lattice QCD* or *flux tube model* say that glue has an extremely important role in QCD. In fact when any model with glue makes predictions about the meson spectrum, a consistent prediction of *gluonic excitations* emerges. Not only do we get the normal $q\bar{q}$ spectrum, but we get additional states which directly involve the gluons. Ones involving only gluons are called *glueballs*, while those that involve gluonic excitations of a $q\bar{q}$ system are known as *hybrids*.

4.1 Glueballs

Naively what is going on? The gluons carry the color charges of QCD, in fact a gluon carries both a color and an anti–color, and are members of an SU(3)–color octet. This leads to eight different gluons. Because these gluons carry color charge, it is possible for them to bind into color singlet objects. In the bag model picture, the simplest glueballs are either two or three gluons confined together as shown in Fig. 6. Currently, the best predictions for the glueball spectrum comes from the lattice. A

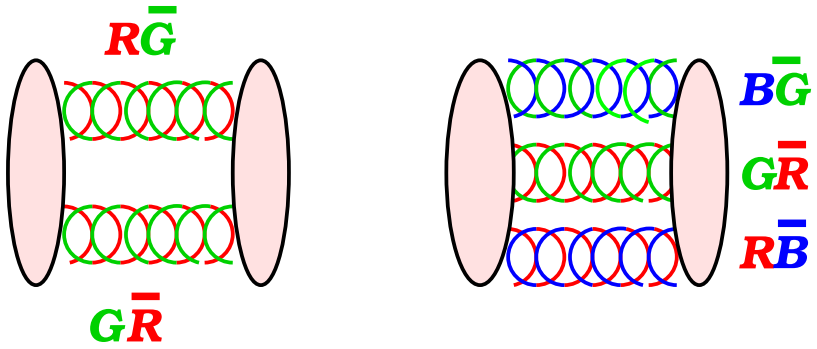

Figure 6: Two and three gluons bound into color singlet glueballs.

recent calculation using and anisotropic lattice [morningstar99] is shown in Fig 7. From this figure, we see that the lightest glueball is expected to have $\mathbf{J^{PC}} = 0^{++}$, followed by a 2^{++} state and then a 0^{-+} state. Unfortunately, all of these quantum numbers are also the quantum numbers of normal mesons. In fact the lightest glueball states with *exotic* or non–$q\bar{q}$ quantum numbers are the 2^{+-} near $4\,\mathrm{GeV/c^2}$ and the 0^{+-} state near $4.5\,\mathrm{GeV/c^2}$. Both well beyond the mass regime that we consider for

light–quark mesons. This means that as far as quantum numbers go, the lightest glueballs will appear to be f_0, f_2 and η states. The main difference is that we expect one additional state beyond the nominal nonets. Worse still, as we have already seen mixing between the two iso–singlet states in a nonet, we should expect that the glueball will also mix into these states as well.

If we first consider the scalar glueball, ($\mathbf{J^{PC}} = 0^{++}$), we find that the lattice prediction for the pure glueball state is $m = (1.6 \pm 0.3)\,\mathrm{GeV/c^2}$. Unfortunately, this is extremely close to the nonet of scalar mesons, $a_0(1450)$, $f_0(1370)$, and $K_0^*(1430)$. This means that it is going to be difficult to establish such a state as a glueball. We will first need to find a 10'th scalar state in the same mass regime. We can also look at the naive predictions for the glueball decay to pairs of pseudoscalar mesons. Under the assumption that the glueball coupling to all pairs of octet mesons are the same, then we obtain that the following relationships.

$$\gamma(G \to \pi\pi) = g_1^g \sqrt{\frac{3}{8}}$$
$$\gamma(G \to \eta_8\eta_8) = -g_1^g \sqrt{\frac{1}{8}}$$
$$\gamma(G \to K\bar{K}) = g_1^g \sqrt{\frac{2}{8}}$$
$$\gamma(G \to \bar{K}K) = -g_1^g \sqrt{\frac{2}{8}}$$

The singlet glueball can also couple to two singlet η's as follows:

$$\gamma(G \to \eta_1\eta_1) = g_{11}^g.$$

We can now expand the possible pairs of physical η and η' states in terms of $\mid \eta_1 >$ and $\mid \eta_8 >$ states as follows.

$$\begin{aligned} \mid \eta > \mid \eta' > &= (\cos\theta_P \mid \eta_8 > - \sin\theta_P \mid \eta_1 >) \cdot (\sin\theta_P \mid \eta_8 > + \cos\theta_P \mid \eta_1 >) \\ &= \sin\theta_P \cos\theta_P (\mid \eta_8 > \mid \eta_8 > - \mid \eta_1 > \mid \eta_1 >) + (\cos^2\theta_P - \sin^2\theta_P) \mid \eta_8 > \mid \eta_1 > \end{aligned}$$

$$\begin{aligned} \mid \eta > \mid \eta > &= (\cos\theta_P \mid \eta_8 > - \sin\theta_P \mid \eta_1 >) \cdot (\cos\theta_P \mid \eta_8 > - \sin\theta_P \mid \eta_1 >) \\ &= \cos^2\theta_P \mid \eta_8 > \mid \eta_8 > + \sin^2\theta_P \mid \eta_1 > \mid \eta_1 > -2\sin\theta_P \cos\theta_P \mid \eta_8 > \mid \eta_1 > \end{aligned}$$

$$\begin{aligned} \mid \eta' > \mid \eta' > &= (\sin\theta_P \mid \eta_8 > + \cos\theta_P \mid \eta_1 >) \cdot (\sin\theta_P \mid \eta_1 > - \cos\theta_P \mid \eta_1 >) \\ &= \cos^2\theta_P \mid \eta_1 > \mid \eta_1 > + \sin^2\theta_P) \mid \eta_8 > \mid \eta_8 > +2\sin\theta_P \cos\theta_P \mid \eta_8 > \mid \eta_1 > \end{aligned}$$

The glueball state is an SU(3) singlet, so it can only couple to $\mid \eta_1 > \mid \eta_1 >$ and $\mid \eta_8 > \mid \eta_8 >$. This leads to the following rates for glueball decay into the physical states:

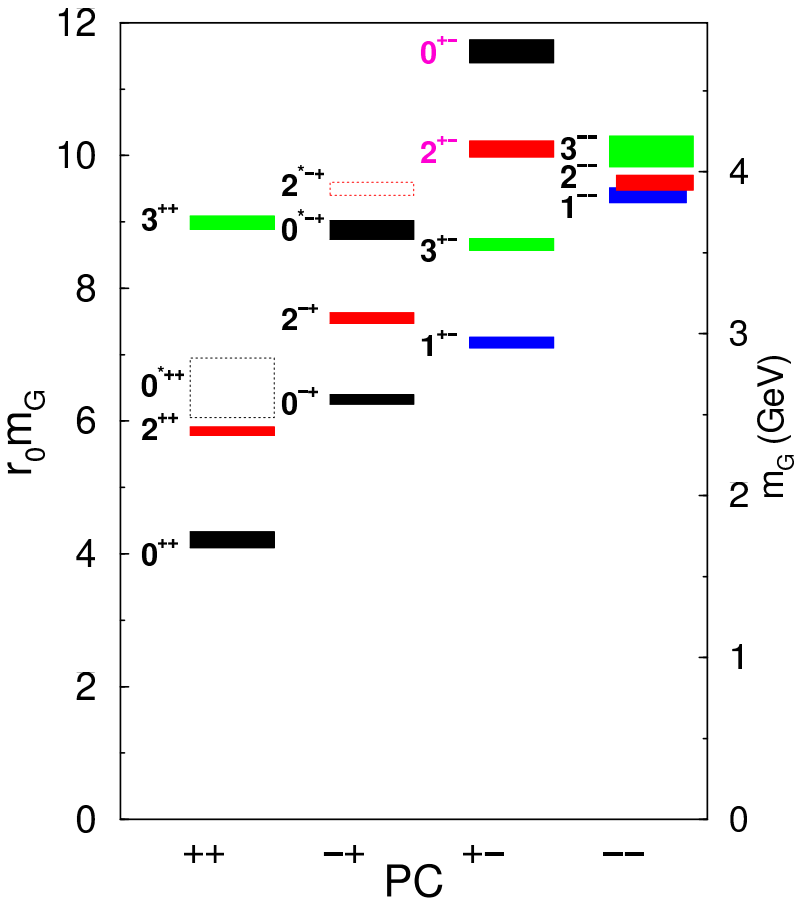

Figure 7: The predicted glueball spectrum from a lattice calculation [morningstar99].

$$\gamma(G \to \eta\eta) = -g_1^g \cos^2\theta_P \sqrt{\frac{1}{8}} + g_{11}^g \sin^2\theta_P$$

$$\gamma(G \to \eta\eta') = \sin\theta_P \cos\theta_P (-\sqrt{\frac{1}{8}} g_1^g - g_{11}^g)$$

$$\gamma(G \to \eta'\eta') = g_{11}^g \cos^2\theta_P - g_1^g \sin^2\theta_P \sqrt{\frac{1}{8}}$$

If we assume that $g_{11}^g = -\sqrt{\frac{1}{8}} g_1^g$, which is equivalent to:

$$\gamma(\mid G > \to \mid \eta_1\eta_1 >) = \gamma(\mid G > \to \mid \eta_8\eta_8 >)$$

then we can can simplify the above rates. Note that in the case of a meson nonet and a pure singlet state decaying to $\eta\eta'$, we would have $g_1 = -\frac{4}{\sqrt{5}} g_T$ for g_1^g and $g_{11} = \sqrt{\frac{2}{5}} g_T$ for g_{11}^g, where it is then clear that $g_{11} = -\sqrt{\frac{1}{8}} g_1$. In general, it is not possible for a pure singlet state to decay into $\eta\eta'$. As such, one would need good reasons for not choosing this, (e.g. the η' has a large glueball component). Simplifying, we obtain that rate for $\eta\eta'$ is zero for any choice of θ_P, and that that rates for $\eta\eta$ and $\eta'\eta'$ are the same for any choice of θ_P. Putting all of this together, we obtain the predictions in 27 as given in [close88]. These are what are typically quoted as the expected flavor independent glueball decays.

$$\Gamma(G \to \pi\pi : K\bar{K} : \eta\eta : \eta\eta' : \eta'\eta') = 3 : 4 : 1 : 0 : 1 \tag{27}$$

In comparing our glueball decays to normal mesons decays, we need to allow for the possibility that the glueball coupling to mesons might be different from that of a meson coupling to other mesons. In this case, we will expand table 5 to 7.

Decay	Constant	Constant/g_T
$\mid 8 > \to \mid 8 > \otimes \mid 8 >$	g_T	1.00
$\mid 8 > \to \mid 8 > \otimes \mid 1 >$	g_{18}	$\sqrt{\frac{2}{5}}$
$\mid 1 > \to \mid 8 > \otimes \mid 8 >$	g_1	$-\frac{4}{\sqrt{5}}$
$\mid 1 > \to \mid 1 > \otimes \mid 1 >$	g_{11}	$\sqrt{\frac{2}{5}}$
$\mid 1 >^g \to \mid 8 > \otimes \mid 8 >$	g_1^g	$-\frac{4}{\sqrt{5}} R$
$\mid 1 >^g \to \mid 1 > \otimes \mid 1 >$	g_{11}^g	$\sqrt{\frac{2}{5}} R$

Table 7: The four SU(3) decay constants for mesons and the two for glueballs expressed in terms of the single constant g_T and a relative strength R between the glueball and meson decays. These constants assume perfect OZI supression.

There is also one lattice calculation which computes glueball decays [sexton95]. They find the mass of the 0^{++} glueball to be $1.740 \pm 0.071\,\mathrm{GeV/c^2}$ and a total width to pairs of pseudoscalar mesons of about $0.1\,\mathrm{GeV/c^2}$.

So we expect to find a 0^{++} glueball near 1.6 GeV/c^2, which is unfortunately rather close to the normal scalar mesons. Where should we look for this object? There are certain production reactions which are considered *glue rich*. Such reactions have a lot of glue, and are considered prime sources of glueballs. There are other reactions which are *glue poor*. In these, some other production mechanism is at play which would suppress the pure glue signal.

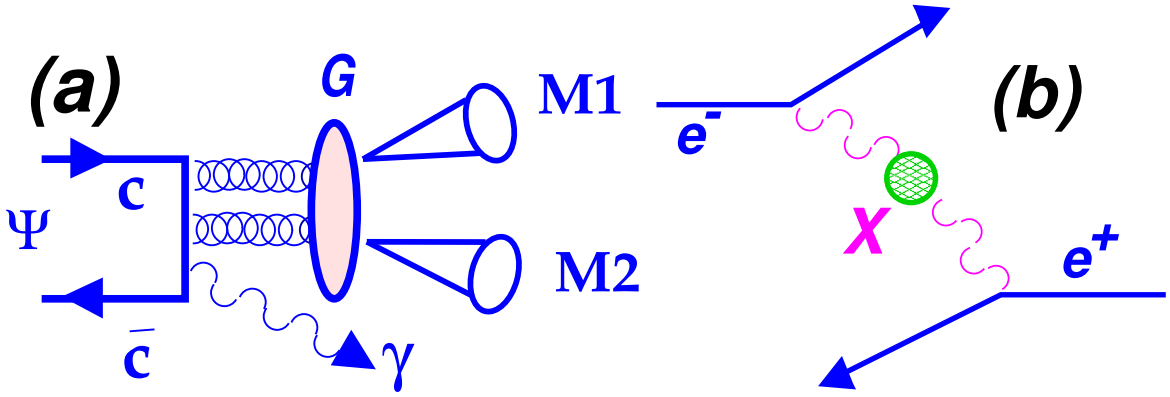

Figure 8: **a**) J/ψ Decay. **(b)** $\gamma\gamma$ fusion.

The best *glue rich* reaction is considered to be radiative J/ψ decays, (Fig. 8a). In this reaction the only mechanism to get from the initial $c\bar{c}$ state to the final state is through intermediate gluons. Typical radiative rates are on the order of 10^{-4} to 10^{-3} with the total radiative width being on order of 6% of all decays. Current existing event samples consist of a few million events, which leads to at most a few thousand events in any one channel. Currently, the only running experiment is BES in Beijing. Their plans are to accumulate on the order of 10^7 J/ψ's within the next couple of years. However, to make significant progress would require a sample of 10^8 to 10^9 events, and would require the construction of a τ–charm factory.

Somewhat related to J/ψ decays is the two–photon fusion process, $\gamma\gamma \to X$ and is considered to be *glue poor*. The photons only couple to electric charge, of which the gluons have none. Both of these reactions are done at e^+e^- machines, so historically they are reactions that could be looked at in the same detector. The basic reaction is shown in Fig. 8b. The idea is that the q^2 of a radiated photon is

$$q^2 = -4E_{\rm beam}E_i \sin^2\frac{\theta_i}{2}.$$

A real photon has q^2 of zero, so by selecting θ_i as close to zero as possible, the process involves two real photons. This is done by **not** seeing the scattered electrons. Currently, there is some effort in the LEP experiments as well as in CLEO to look at two–photon production of mesons. The most recent review [cooper88] is fairly old.

The two–photon production couples to the electric charge of a meson, while the radiative J/ψ decays couple to the color charge of a meson. One can define a quantity known as the *stickiness*, (equation 28), which is essentially the ratio of the color charge

to the electric charge of a state [chanowitz84].

$$S = N \cdot \frac{m_x}{(m_\psi^2 - m_x^2)/2m_\psi} \cdot \frac{\Gamma(\psi \to \gamma X)}{\Gamma(X \to \gamma\gamma)} \tag{28}$$

This quantity is normalized to be one for the $f_2(1270)$ which is believed to be a pure $q\bar{q}$ state. One would expect that S would be large for states which are gluonic in nature.

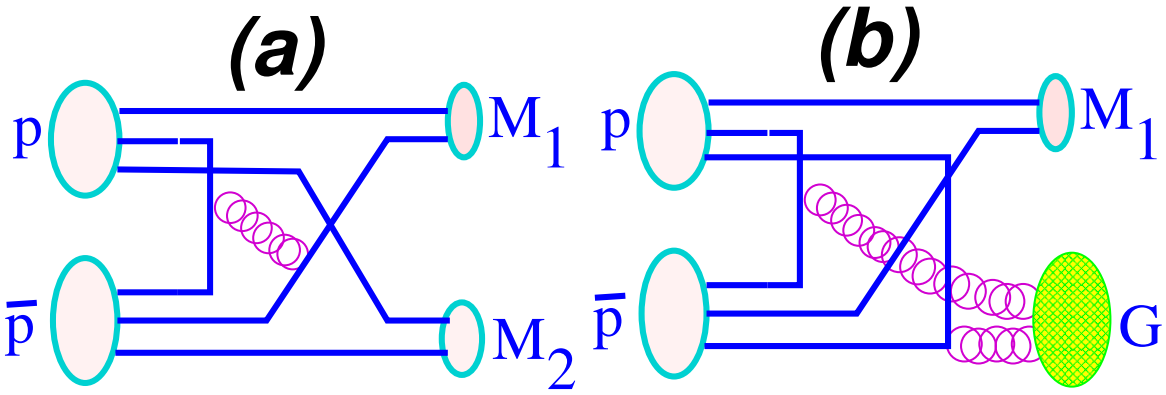

Figure 9: Proton–antiproton annihilation into **(a)**meson pairs and **(b)** gluonic final states.

A second reaction which is considered *glue–rich* is proton–antiproton annihilation. Typical annihilation to mesons proceeds via a quark rearrangement as shown in Fig. 9a. However, as there is expected to be a lot of gluons, a reaction such as Fig. 9b. is also expected to play an important role. A large amount of data has been recently accumulated at the Low Energy Antiproton Ring, LEAR, at CERN. Particularly with the Crystal Barrel experiment, see the very recent review by Amsler [amsler98]. For $\bar{p}p$ annihilations at rest, which experimentally are a very good source of scalars, one is limited to $\sqrt{s} = 2m_p - m_\pi$, or about $1.74\,\mathrm{GeV/c^2}$.

A final place which is considered to be *glue rich* are in central production reactions, (see Fig. 10a). Essentially the two initial state particles leave the reaction as the same state, while the meson, X, is created in the exchange of two virtual particles of momentum transfer q_1 and q_2. For large enough energies, this reaction tends to be dominated by diffractive processes, which in turn appear to be dominated by so called *pomeron* exchange. The nature of the pomeron is not clear, but it is believed to have a significant gluonic nature. This means that a double pomeron exchange would be a very good place to look for gluonic excitations.

Finally, another nominally *glue poor* reaction is photoproduction, (see Fig. 10b). This is suppressed due the fact that the photon couples to electric charge. However, it may not be as suppressed as the $\gamma\gamma$ reactions.

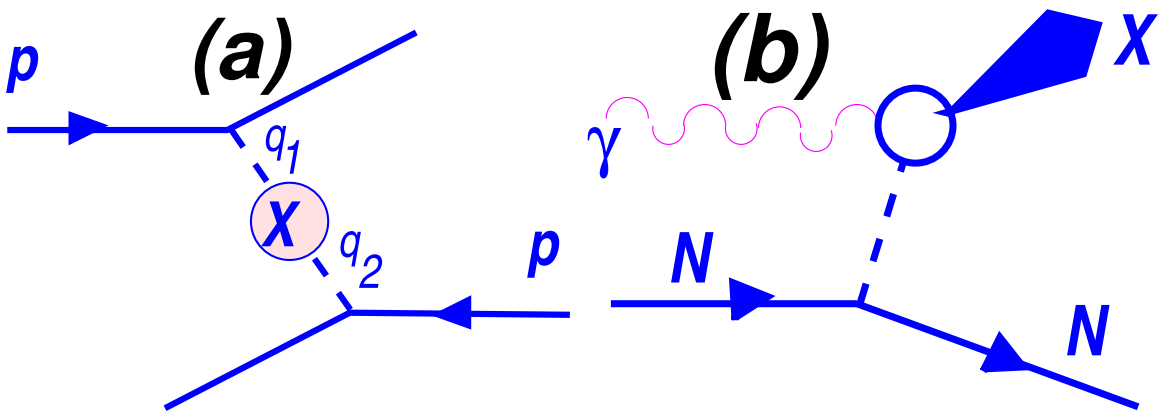

Figure 10: **(a)**Central Production, **(b)** Photo Production.

4.2 Hybrids

Not only can we consider purely glue states, but one could imagine the gluons contributing directly to the quantum numbers of the system, *valance glue*. These states, $(q\bar{q}g)$ are know as *hybrid mesons* or *hybrids*. A picture of what is actually

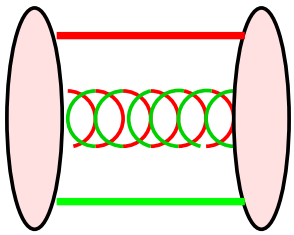

Figure 11: Hybrid Meson

happening is related to the self-interaction of the gluon field within a meson. In the upper part of Figure 12 is shown the flux lines for Coulomb like force. The lines expand to fill all space, and using Gauss's law, we arrive at a $1/r^2$ fall off for the force. In the case of QCD, the gluons in the color field attract each other. The resulting flux lines are shown in the lower part of Figure 12 [bali98]. The lines are confined to some narrow region of space between the quark and antiquark. Using Gauss's law for this field configuration, one obtains a force between the quark and the antiquark that is independent of distance between them. As one starts to separate the two, the energy required rises linearly with separation until eventually enough energy has been added such that a new quark-antiquark pair is created from the vacuum. This is shown in Figure 13. This notion of the formation of flux tubes was first introduced in the 1970's by Yoichiro Nambu [nambu70, nambu76] to explain the observed linear Regge trajectories – the linear dependence of mass squared, m^2, of hadrons on their spin, J. This linear dependence results if one assumes that massless quarks are tied to the ends of a relativistic string with constant mass (energy) per length with the system

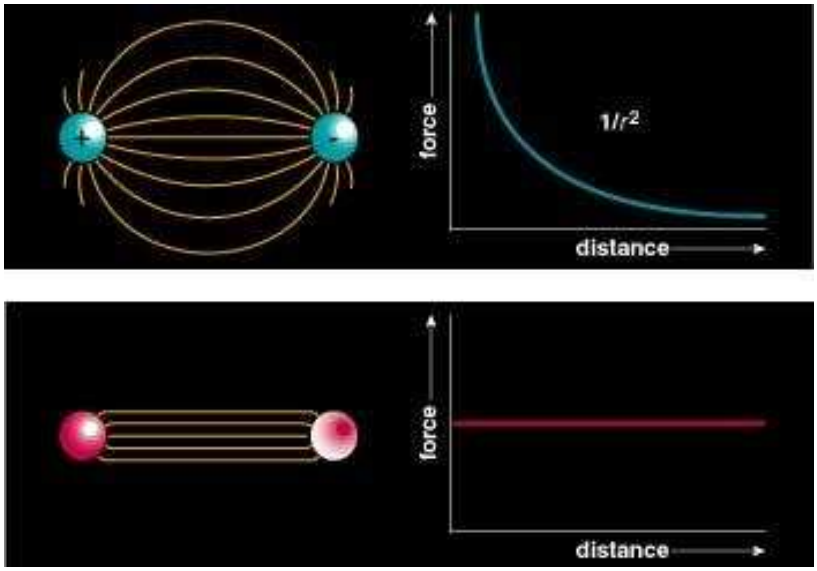

Figure 12: Field lines associated with the electrical force between two electrically charged particles (top) and the corresponding dependence of force on the distance between the charges and the field lines associated with the color force (bottom) between two quarks and the corresponding dependence of force on distance.

rotating about its center. The linear m^2 versus J dependence only arises when the mass density per length is constant, which is equivalent to a linear potential.

This interpretation, which is known as the *flux tube model* has been confirmed in the heavy quark sector using lattice QCD. In Figure 14 is shown the energy density in the color field between a static quark and anti-quark pair. The region between the two quarks is the formation of a flux tube. Also shown is the potential between the quark anti-quark pair. The linear rise at larger r is due to the constant force prodeuce by the flux tube. The higher potentials correspond to exictations of the flux tube itself, and bound staes of these excited potentials would correspond to hybrid mesons.

Within the *flux tube model* [isgur85], one can view *hybrids* as mesons with angular momentum in the flux tube. Naively, one can imagine two degenerate excitations, one with the tube going clockwise and one counter clockwise. It is possible to write linear combinations of these that have definite spin, parity and C-parity. For the case of one unit of angular momentum in the tube, we have $J^{PC} = 1^{+-}$ and 1^{-+}. The basic quantum numbers of hybrids can then be obtained by adding the tube's quantum numbers to that of the underlying meson. In the model, the flux–tube carries angular momentum, m, which then leads to specific **CP** predictions. For $m = 0$, $\mathbf{CP} = (-1)^{S+1}$, while for the first excited states, $m = 1$, $\mathbf{CP} = (-1)^{S}$. The excitations are then built on top of the S–wave mesons, $(L = 0)$, where the total spin can be either $\mathbf{S} = 0$ or $\mathbf{S} = 1$. These lead to the expected quantum numbers for $m = 0$ and $m = 1$; in this picture the $m = 0$ are the normal quark–model mesons, while the

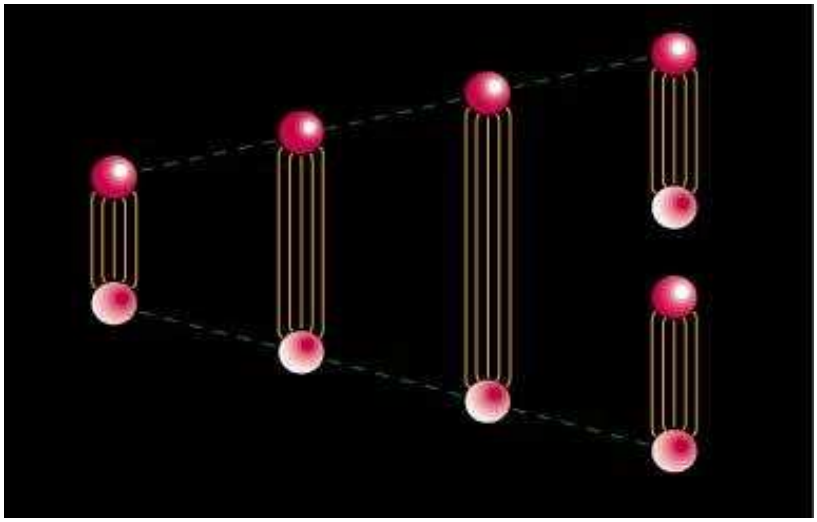

Figure 13: As the $q\bar{q}$ pair is separated, the enrgy in the gluonic tube eventually becomes so large that a new $q\bar{q}$ pair is created.

$m = 1$ are the lowest lying hybrid mesons.

$$(m=0)\ \left.\begin{array}{l} S=0\ 0^{-+} \\ S=1\ 1^{--} \end{array}\right\}\ \begin{array}{c} (-1)^{L+1}(-1)^{S+L} = (-1)^{S+1} \\ \text{Normal Mesons} \end{array}$$

$$(m=1)\ \left.\begin{array}{l} S=0\ 0^{-+} \\ S=1\ 1^{--} \end{array}\right\}\ \begin{array}{c} 1^{++}, 1^{--} \\ 0^{-+}, \mathbf{0}^{+-}, \mathbf{1}^{-+}, 1^{+-}, 2^{-+}, \mathbf{2}^{+-} \end{array}$$

The $m = 1$ predictions are obtained by adding both 1^{+-} and 1^{-+} to the quark quantum numbers of either 0^{-+} or 1^{--}. We also note that for the two $S = 0$ nonets in the quark model, we have eight hybrid nonets, (72 new mesons!), and that three of the eight nonets (indicated in bold) have non–$q\bar{q}$, or exotic quantum numbers. In this picture, these hybrids are no different than the excitations of the $q\bar{q}$ states, we just need to consider *Orbital*, *Radial*, and *Gluonic* excitations as the natural degrees of freedom. In Fig 15 are shown the approximate expectations for the quark model states, $q\bar{q}$, the glueballs, the lightest hybrids, and where some two–meson thresholds are.

Within the flux-tube model, all eight hybrid nonets are degenrate. However, lattice QCD calculations indicate that the exotic 1^{-+} nonet is likely to be the lightest.

In the sense that hybrid mesons are just excitations of the gluon field, they should be produced in all reactions which populate the excited $q\bar{q}$ spectrum. However, it is believed that the spin of the initial particle will likely be transfered directly into the spin of the $q\bar{q}$ system in the hybrid. This means that beams of π's and K's are likely to produce hybrids built on spin zero objects, 1^{--} and 1^{++}. Similarly, beams of spin one particles are more likely to produce hydrids built on spin-alligned quarks, 0^{+-}, 0^{-+}, 1^{+-}, 1^{-+}, 2^{+-} and 2^{-+}. Hybrids should in principal be produced as strongly as other states.

Predictions for the widths of hybrids are currently based on model calculations

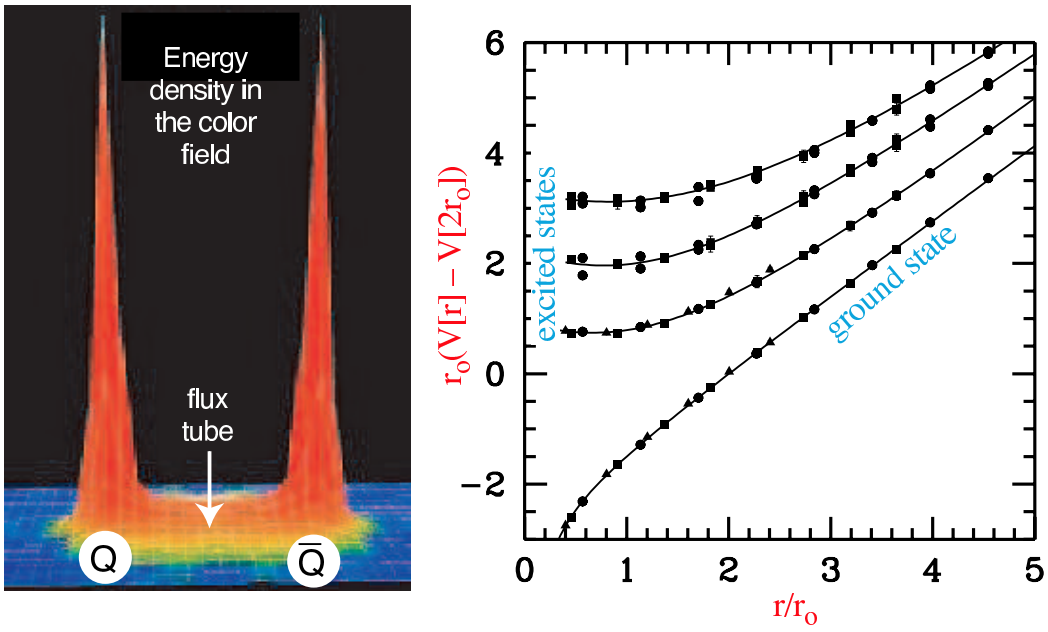

Figure 14: (left) A lattice QCD calculation of the energy density in the color field between a quark and an anti-quark. The density peaks at the positions of the quarks and is confined to a tube between the quarks. This calculation is for heavy quarks in the quenched approximation. (right) The corresponding potential between the quarks. The ground state potential has a $1/r$ dependence at small distances and is linear for large distances.

Light Quark 1^{-+}		Charmonium 1^{-+}	
Reference	Mass GeV/c^2	Reference	ΔM GeV/c^2
UKQCD [lacock97]	1.87 ± 0.20	MILC [bernard97]	$1.34 \pm 0.08 \pm 0.20$
MILC [bernard97]	$1.97 \pm 0.09 \pm 30$	MILC [bernard99]	1.22 ± 0.15
MILC [bernard99]	2.11 ± 0.13	[manke-99]	1.323 ± 0.130
LaSch [lacock99]	1.9 ± 0.20	[juge99]	1.19
[zhong02]	$2.013 \pm 0.026 \pm 0.071$		

Table 8: Recent results for the light-quark and charmonium 1^{-+} hybrid meson masses. For the charmonium spectrum, the difference is taken from the $1S$ state. The table is based on a similar table in [morningstar01].

with the most recent work [page99] given in Table 9 for states with exotic quantum numbers, and in Table 10 for hybrids with normal $q\bar{q}$ quantum numbers. As can be seen, a number of these states are expected to be broad. In particular, most of the 0^{+-} exotic nonet are quite borad. However, states in both the 2^{+-} and the 1^{-+} nonets have much narrower expected widths. The normal quantum numbers states will be more difficult to disentangle as they are likely to mix with nearby normal $q\bar{q}$ statess. Finally, the expected decay modes of these states involve daughters that in turn decay. This makes the overall reconstruction more complcated then simple

Particle	$\mathbf{J^{PC}}$	Total Width MeV		Large Decays
		[page99]	[isgur85a]	
π_1	1^{-+}	$81-168$	117	$b_1\pi$, $\rho\pi$, $\eta(1295)\pi$
η_1	1^{-+}	$59-158$	107	$a_1\pi$, $\pi(1300)\pi$
η_1'	1^{-+}	$95-216$	172	$K_1(1400)K$, $K_1(1270)K$, K^*K
b_0	0^{+-}	$247-429$	665	$\pi(1300)\pi$, $h_1\pi$
h_0	0^{+-}	$59-262$	94	$b_1\pi$
h_0'	0^{+-}	$259-490$	426	$K(1460)K$, $K_1(1270)K$
b_2	2^{+-}	$5-11$	248	$a_2\pi$, $a_1\pi$, $h_1\pi$
h_2	2^{+-}	$4-12$	166	$b_1\pi$, $\rho\pi$
h_2'	2^{+-}	$5-18$	79	$K_1(1400)K$, $K_1(1270)K$, $K_2^*(1430)K$

Table 9: Exotic quantum number hybrid width and decay predictions.

peseudoscalar mesons.

However, these decays can be used as a guideline when looking for these states. Almost all models of hybrid mesons predict that the ground state ones will not decay to identical pairs of mesons, and that the decays to an $(L=0)(L=1)$ pair is the favored decay mode. Essentially, the one unit of angular momentum in the flux–tube has to go into internal orbital angular momentum of a $q\bar{q}$ pair. In addition, the nonet with non $q\bar{q}$ quantum numbers provide a striking signal for these objects. It is also true that lattice calculations predict that the 1^{-+} nonet, (exotic) is the lightest (see table 8). Above this, the exotic 0^{+-} and the 2^{+-} are the next lightest. It is also important to keep in mind that the splittings between nonets is due to the gluonic degrees of freedom, so a measurement of this quantity can provide insight into the confining potential of QCD.

Particle	$\mathbf{J^{PC}}$	Total Width MeV		Large Decays
		[page99]	[isgur85a]	
ρ	1^{--}	$70-121$	112	$a_1\pi$,$\omega\pi$, $\rho\pi$
ω	1^{--}	$61-134$	60	$\rho\pi$, $\omega\eta$, $\rho(1450)\pi$
ϕ	1^{--}	$95-155$	120	$K_1(1400)K$, K^*K, $\phi\eta$
a_1	1^{++}	$108-204$	269	$\rho(1450)\pi$, $\rho\pi$, K^*K
h_1	1^{++}	$43-130$	436	K^*K, $a_1\pi$
h_1'	1^{++}	$119-164$	219	$K^*(1410)K$,K^*K
π	0^{-+}	$102-224$	132	$\rho\pi$,$f_0(1370)\pi$
η	0^{-+}	$81-210$	196	$a_0(1450)\pi$, K^*K
η'	0^{-+}	$215-390$	335	K_0^*K,$f_0(1370)\eta$, K^*K
b_1	1^{+-}	$177-338$	384	$\omega(1420)\pi$,K^*K
h_1	1^{+-}	$305-529$	632	$\rho(1450)\pi$, $\rho\pi$, K^*K
h_1'	1^{+-}	$301-373$	443	$K^*(1410)K$, $\phi\eta$, K^*K
π_2	2^{-+}	$27-63$	59	$\rho\pi$,$f_2\pi$
η_2	2^{-+}	$27-58$	69	$a_2\pi$
η_2'	2^{-+}	$38-91$	69	K_2^*K, K^*K

Table 10: Non-exotic quantum number hybrid width and decay predictions.

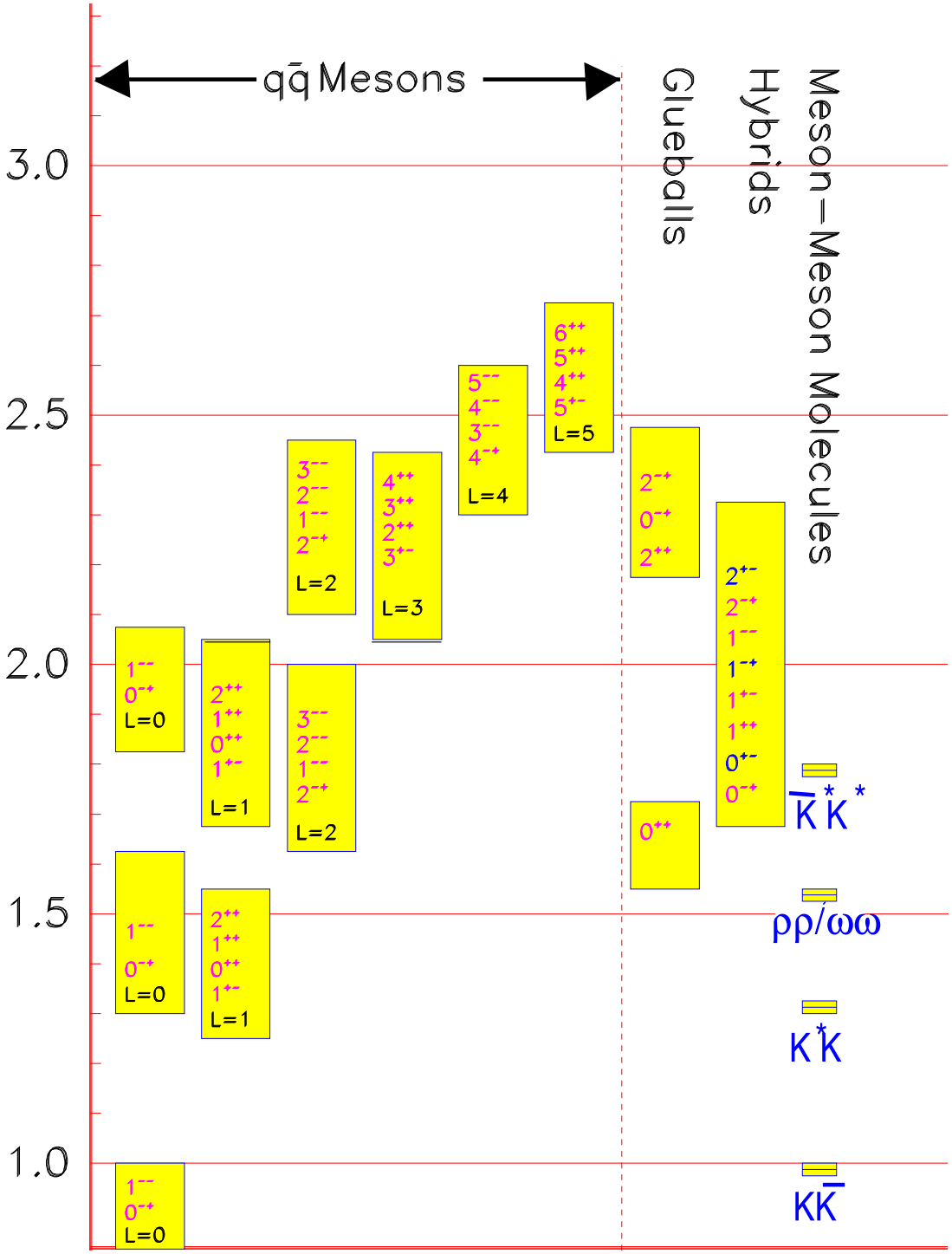

Figure 15: The expected mesons spectrum. For the $q\bar{q}$

5 Partial Wave Analysis

Partial wave analysis is a technique which attempts to fit the production and subsequent decay of a meson by examining not only its mass distribution, but also all angular distributions of the system. The technique is very powerful, but requires rather large statistics to be able to identify things.

5.1 The Resonance Shape

Strongly decaying particles have lifetimes on the order of 10^{-23} seconds which, through the uncertainty principle, leads to widths on the order of $100\,\mathrm{MeV/c^2}$. If we had an isolated state of mass m_0 and width Γ_0, then we would describe the resonance in terms of a Breit–Wigner amplitude as in 29.

$$\mathrm{BW}(m) = \frac{\Gamma_0/2}{m_0 - m - i\Gamma_0/2} \tag{29}$$

This form is the non–relativistic form, and is valid when $\Gamma_0 << m_0$, and the mass m_0 is far from the threshold for the decay. This can be extended to the so called relativistic form as given in 30. In this form, the resonance shape depends on the relative angular momentum, L, with which the resonance is produced. In addition, the width, $\Gamma(m)$ depends on the orbital angular momentum l between the daughter products, as well as phase space available to them.

$$\mathrm{BW}_L(m) = \frac{m_0\Gamma(m)}{m_0^2 - m^2 - im_0\Gamma(m)} \tag{30}$$

$$\Gamma(m) = \Gamma_0 \frac{m_0}{m}\frac{p}{p_0}\frac{F_l^2(p)}{F_l^2(p_0)} \tag{31}$$

The angular momentum barrier factors are computed as a function of $z = (p/p_R)^2$, ($p_R = 197\,\mathrm{MeV/c}$), and are given as follows:

$$F_0(p) = 1$$

$$F_1(p) = \sqrt{\frac{2z}{z+1}}$$

$$F_2(p) = \sqrt{\frac{13z^2}{(z-3)^2 + 9z}}$$

$$F_3(p) = \sqrt{\frac{277z^3}{z(z-15)^2 + 9(2z-5)^2}}$$

The shapes are quite similar if both the width of the resonance and the mass of its daughter particles are small compared to its mass. In Fig. 16 are shown a comparison of equation 29 and 30 for several different situations. In **a** is shown the normal ρ mesons, where $m_0 = 0.770\,\mathrm{GeV/c^2}$, $\Gamma_0 = 0.150\,\mathrm{GeV/c^2}$, and both daughter particles

are pions with mass $m = 0.140\,\mathrm{GeV/c^2}$. In **b**, we have let the daughter particles have mass $m = 0.350\,\mathrm{GeV/c^2}$, and one can easily see the threshold effect of the two daughters. Finally, in **c**, the width has been changed to $\Gamma_0 = 0.350\,\mathrm{GeV/c^2}$.

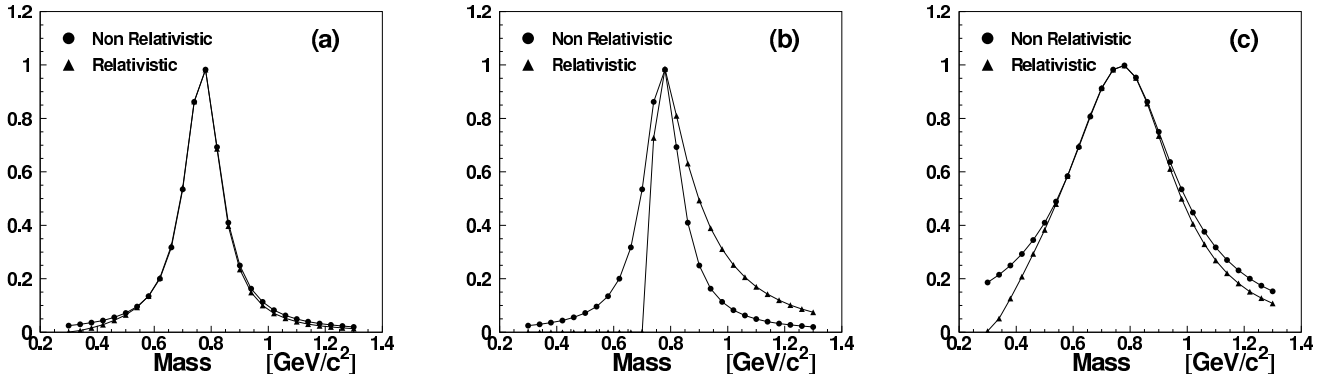

Figure 16: A comparison of the relativistic and non relativistic resonance shapes for a ρ meson under different assumptions. **a** $m_\rho = 0.770\,\mathrm{GeV/c^2}$, $\Gamma_\rho = 0.150\,\mathrm{GeV/c^2}$ and $m_1 = m_2 = 0.140\,\mathrm{GeV/c^2}$. **b** $m_\rho = 0.770\,\mathrm{GeV/c^2}$, $\Gamma_\rho = 0.150\,\mathrm{GeV/c^2}$ and $m_1 = m_2 = 0.350\,\mathrm{GeV/c^2}$. **c** $m_\rho = 0.770\,\mathrm{GeV/c^2}$, $\Gamma_\rho = 0.350\,\mathrm{GeV/c^2}$ and $m_1 = m_2 = 0.140\,\mathrm{GeV/c^2}$.

A second issue is what are quoted as the mass and width of a resonance? Usually, one will quote a complex value of m, $(m = m_R - i\Gamma_R/2)$, such that the amplitude has a pole at that value. For the case of 29, it is easy to see that if $m_R = m_0$ and $\Gamma_R = \Gamma_0$, that there is indeed a pole. However, in the relativistic form in 30, it is rather obvious that m_0 and Γ_0 will not produce a pole, though they are not very far off for many cases. There are also other things which are quoted. The mass which makes the amplitude purely complex is one such possibility. Another is the mass that yields the maximum rate of change in the amplitude. Because of this, the values which are quoted in literature tend to have a wide variety of meanings. In my mind, the most logical value to quote is the so called *T–matrix poles*. In scattering theory, one considers an S–matrix which takes an initial state to a final state,

$$S_{fi} = < f \mid S \mid i >$$

such that the S matrix is unitary, $SS^\dagger = I$. We can rewrite the S in terms of the T–matrix as $S = I + 2iT$ where the T matrix can be written in terms of a scattering phase as $T = e^{i\delta} \sin\delta$. This is discussed in more detail in section 5.3.

5.2 The Angular Distributions

By fitting Breit–Wigner forms to the data, we can in principle learn the masses and widths of a state. However, we are unable to determine the $\mathbf{J^{PC}}$ of a state. In

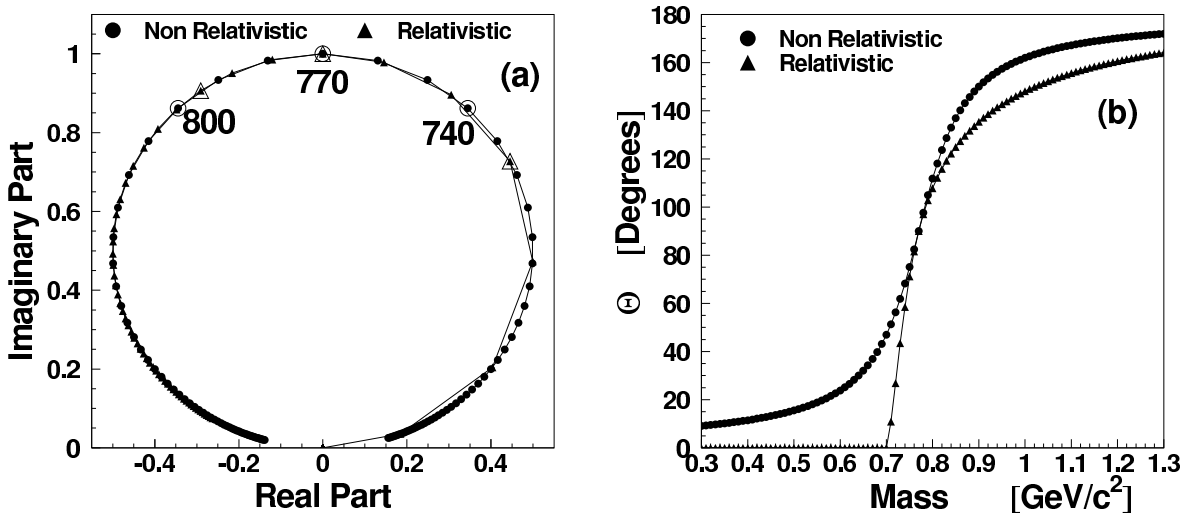

Figure 17: **a** The imaginary versus the real part of the Breit–Wigner amplitude for the $\rho(770)$. **b** The phase δ as a function of mass for the $\rho(770)$. Non relativistic corresponds to equation 29 while relativistic corresponds to equation 30.

order to do this, we have to look at the angular distributions of the decay products with respect to some initial state. It is the fitting of these distributions which is referred to as a *partial wave analysis*. There are two forms by which one normally constructs these angular distributions. The Zemach Tensors [zemach64] and the Helicity formalism [jacobs59]. An excellent reference on this has been written by Richman [richman84]. They both work equally well for many problems, but we will only discuss the latter in this work. Let us consider the decay of particle **A** with mass m_A and spin J_A into two daughter particles, **B** and **C**. These have masses m_B and m_C, and spins S_B and S_C respectively. We will look at the system from the rest frame of **A**. If there is no preferred direction in this system, then we are free to choose the direction of the z axis to be along the direction of one of the daughter particles. (Actually, even if there is some preferred direction, we can always rotate the system such that the z axis is aligned so.) We will also allow the two daughter particles to have relative orbital angular momentum L.

$$\mathbf{A}(m_A, J_A) \rightarrow \underbrace{\mathbf{B}(m_B, S_B) + \mathbf{C}(m_C, S_C)}_{L}$$

Using z as our quantization axis, then there are $2J_A + 1$ initial states and $(2S_B + 1)(2S_C + 1)$ final states possible. Our job is to consider the transitions from the initial to the final states. If we now write these in terms of momentum helicity states, then

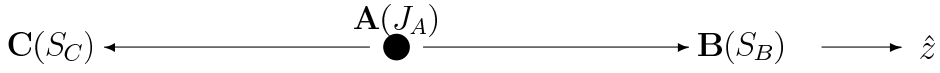

the final states can be referenced as $\mid p, \lambda_B, \lambda_C >$ where p is the momentum of particle **B**, and the λ's are the helicities of the two daughters. The helicity is defined as the projection of the total spin, J, along the direction of the particle. Using the fact that $\vec{L}$ and $\vec{p}$ are normal to each other, we arrive at:

$$\lambda = \frac{\vec{J}\cdot\vec{p}}{\mid\vec{p}\mid} = \frac{\vec{l}\cdot\vec{p}}{\mid\vec{p}\mid} \oplus \frac{\vec{s}\cdot\vec{p}}{\mid\vec{p}\mid} = 0 + m_S, \tag{32}$$

where m_S is just the projection of the particles spin along the z axis. This means that $\lambda_B = m_s(B)$ and $\lambda_C = -m_s(C)$. Now we can generalize this to **B** being emitted in some arbitrary direction, (θ, ϕ), rather than simply along the $\hat{z}$ axis. We can get from this new frame back to the frame where **B** is moving along the z axis via a rotation in three space, $R(\theta, \phi) = R_{y_2}(\theta)R_{z_1}(\phi)$. We may recall that when doing classical rotations, we used three Euler angles to accomplish the rotation of a reference frame. The third would be a rotation about the direction of particle **B**, which in the case of a spin-less particle is not needed, (only two angles are needed to rotate a vector). It should however be noted that if the final state particle has non–zero spin, it is necessary to perform a third rotation to align the polarization vectors. Rotations can be expressed as a unitary operator,

$$(U(\alpha, \beta, \gamma) = R_z(\gamma)R_y(\beta)R_z(\alpha) = e^{-iJ_z\alpha}e^{-iJ_y\beta}e^{-iJ_z\gamma}$$

where the convention is based on the Euler angles α, β, γ. Using this, we can rotate some state $\mid j, m\rangle$ as follows:

$$\begin{aligned} R(\alpha\beta\gamma) \mid j, m\rangle &= \sum_{m'=-j}^{j} D^j_{m'm}(\alpha\beta\gamma) \mid j, m'\rangle \\ \langle j, m'' \mid R(\alpha\beta\gamma) \mid j, m\rangle &= \sum_{m'=-j}^{j} D^j_{m'm}(\alpha\beta\gamma)\langle j, m'' \mid j, m'\rangle \\ &= D^j_{m''m}(\alpha\beta\gamma) \end{aligned}$$

From this, we can now compute the D-function:

$$D^j_{m'm}(\alpha\beta\gamma) = \langle j, m' \mid e^{-iJ_z\alpha}e^{-iJ_y\beta}e^{-iJ_z\gamma} \mid j, m\rangle$$

which can be written as:

$$D^j_{m'm}(\alpha\beta\gamma) = e^{-i\alpha m'}d^j_{m'm}(\beta)e^{-i\gamma m}.$$

The little-d-function is $d^j_{m'm}(\beta) = \langle j, m' \mid e^{-i\beta J_y} \mid j, m\rangle$. The d–functions are elements of a rotation matrix, and can be looked up in several sources [caso98]. For a given j, there are relations between the elements given as in equation 33.

$$d^j_{m'm}(-\beta) = (-1)^{m'-m}d^j_{m'm}(\beta) \tag{33}$$

$$d^j_{m'm}(\beta) \quad = d^j_{-m-m'}(\beta) \quad = (-1)^{m'-m}d^j_{mm'}(\beta) \tag{34}$$

$$\tag{35}$$

These operators can now be used to manipulate one-particle helicity wave functions. If we start with a massive particle at rest with spin s and sping projection λ along the z axis, $\mid \vec{p}=0,s,\lambda\rangle$. Then to obtain the state $\mid \vec{p},s,\lambda\rangle$, we first rotate it so that the quantization axis points along the direction of $\vec{p}$, $\hat{p}(\theta,\phi)$ and then do a Lorentz boost along $\hat{p}$.

$$\mid \vec{p},s,\lambda\rangle = L(\vec{p})R(\alpha\beta\gamma) \mid \vec{p}=0,s,\lambda\rangle$$

There are now two common conventions for choosing α, β and γ. Jacob and Wick [jacobs59] choose $\alpha=\phi$, $\beta=\theta$, and $\gamma=-\phi$, while Chung [chung71] chooses $\alpha=\phi$, $\beta=\theta$ and $\gamma=0$. The choice is just a matter of convenience, and doe not affect the final answer.

So, applying these to our particle, we can rotate our helicity state from system 3 where $\mathbf{B}$ is moving along the $\hat{z}$ axis to system 1 where it is moving in some direction (θ,ϕ).

$$\mid p,\theta,\phi,\lambda_b,\lambda_c,M\rangle = \mathcal{D}^J_{M\lambda}(\phi,\theta,0) \mid p,\lambda_b,\lambda_c\rangle$$

where we have taken the convention of Chung. We are now interested in the general transition amplitude from some initial state $\mid J,M\rangle$ to our final state where the two daughters have helicities λ_1 and λ_2. This can be written as a transition matrix, f as follows.

$$\begin{aligned} f_{\lambda_1,\lambda_2,M}(\theta,\phi) &= \langle p,\theta,\phi,\lambda_1,\lambda_2,M' \mid T \mid M\rangle & (36)\\ &= D^{*J}_{M\lambda}(\phi,\theta,0)\langle\lambda_1\lambda_1 \mid T \mid M> . & (37)\\ & & (38)\end{aligned}$$

This is a matrix with $(2J+1)$ columns corresponding to the initial states, and $(2S_1+1)(2S_2+1)$ rows corresponding to the final states. The T_{λ_1,λ_2} are formed by summing over all possible l and s values with an unknown complex coefficient, α_{ls} for each one.

$$T_{\lambda_1,\lambda_2} = \sum_{ls} \alpha_{ls}\langle J,\lambda \mid l,s,0,\lambda\rangle\langle s\lambda \mid S_1,S_2,\lambda_1,-\lambda_2\rangle \qquad (39)$$

This is non–zero only if $\lambda=\lambda_1-\lambda_2$. If the initial state now has a density matrix, ρ_i, ($(2J+1)\times(2J+1)$), then the density matrix of the final state, ρ_f is computed as:

$$\rho_f = f\rho_i f^\dagger$$

The angular distribution of the final state is then obtained by taking the trace of ρ_f,

$$\mathrm{w_D}(\theta,\phi) = \mathrm{Tr}(\rho_f) = \mathrm{Tr}(f\rho_i f^\dagger). \qquad (40)$$

What we have done allows us to handle simple decays into two daughter particles, but it can easily be extended to more complicated decay chains. Let us consider the decay:

$$A \to [B \to B_1B_2]\,[C \to C_1C_2]\,.$$

We can write a transition matrix, f for each of the three decays, $f(A \to BC)$, $f(B \to B_1B_2)$ and $f(C \to C_1C_2)$. The total transition matrix, f_T can then be written as a tensor product of the individual transition matrices.

$$\begin{aligned} f_T &= [f(B) \otimes f(C)] \otimes f(A) \\ &= \sum_{\lambda(B),\lambda(C)} \left\{ \underbrace{f_{\lambda(B_1)\lambda(B_2),\lambda(B)}}_{\theta_B,\phi_B} \otimes \underbrace{f_{\lambda(C_1)\lambda(C_2),\lambda(C)}}_{\theta_C,\phi_C} \right\} \underbrace{f_{\lambda(B)\lambda(C),\lambda(A)}}_{\theta,\phi} \end{aligned}$$

For convenience, the nine d-functions of order 1 are given below.

$$\begin{array}{lll} d^1_{11}(\theta) = \frac{1+\cos\theta}{2} & d^1_{10}(\theta) = -\frac{\sin\theta}{\sqrt{2}} & d^1_{1-1}(\theta) = \frac{1-\cos\theta}{2} \\ d^1_{01}(\theta) = \frac{\sin\theta}{\sqrt{2}} & d^1_{00}(\theta) = \cos\theta & d^1_{0-1}(\theta) = -\frac{\sin\theta}{\sqrt{2}} \\ d^1_{-11}(\theta) = \frac{1-\cos\theta}{2} & d^1_{-10}(\theta) = \frac{\sin\theta}{\sqrt{2}} & d^1_{-1-1}(\theta) = \frac{1+\cos\theta}{2} \end{array}$$

Let us now look at a simple example. We will take proton–antiproton annihilation from an initial atomic $^1S_0$ state into $\rho\pi$. The ρ will then decay into two pions. The decay chain is as shown below, we see that in order to conserve angular momentum, the orbital angular momentum between the ρ and the π must be $L = 1$.

$$^1S_0(\bar{p}p) \to \underbrace{\rho^{\pm}}_{\to\pi^{\pm}\pi^{\circ}} \pi^{\mp} \quad 0^{-+} \to \underbrace{1^-0^-}_{L=1}$$

We now identify **A** as the $\bar{p}p$ state, **B** as the $\rho^{\pm}$ and **C** as the $\pi^{\mp}$. We have $J_A = 0$, $S_B = 1$, $S_C = 0$, and $S = 1$. This means that our transition matrix will have one column (corresponding to J) and three rows, (corresponding to $(2S_B + 1)(2S_C + 1)$). The transition elements are now given as in equation 39. We see that since $J = 0$, the only non–zero elements will have $\lambda = 0$, in addition $\lambda_\rho = 1, 0, -1$ and $\lambda_\pi = 0$. From this, we see that $T_{10} = T_{-10} = 0$ and that

$$T_{00} = \underbrace{\langle 00 \mid 1100 \rangle}_{-1/\sqrt{3}} \underbrace{\langle 10 \mid 1000 \rangle}_{1}$$

so the amplitude for the transition to $\rho\pi$ is

$$f(\to \rho\pi) = T_{\lambda_1\lambda_2} \mathcal{D}^{*J}_{m\lambda}(\phi, \theta, 0)$$

$$f(\to \rho\pi) = \begin{pmatrix} 0 \\ -\frac{1}{\sqrt{3}} \mathcal{D}^{*0}_{00}(\phi, \theta, 0) \\ 0 \end{pmatrix} = \begin{pmatrix} 0 \\ -\frac{1}{\sqrt{3}} \\ 0 \end{pmatrix}$$

Next, we need to consider the decay of $\rho \to \pi\pi$. Here we have $J = 1$ for the ρ, and $S = S_1 = S_2 = 0$ for the π's. Both λ_1 and λ_2 are zero, which means that we only $\lambda = 0$ contributes. This means that $L = 1$, and leads to:

$$T_{\lambda_1\lambda_2} = \langle 1\lambda \mid 100\lambda \rangle < \langle 0\lambda \mid 00\lambda_1 - \lambda_2 \rangle$$

$$T_{00} = \langle 10 \mid 1000 \rangle \langle 00 \mid 0000 \rangle = 1$$

$$f(\rho \to \pi\pi) = \left(\mathcal{D}^{*1}_{10}(\phi_\rho, \theta_\rho, 0)\, \mathcal{D}^{*1}_{00}(\phi_\rho, \theta_\rho, 0)\, \mathcal{D}^{*1}_{-10}(\phi_\rho, \theta_\rho, 0) \right)$$

$$f_T = -\tfrac{1}{\sqrt{3}} \mathcal{D}^{*1}_{00}(\phi_\rho, \theta_\rho, 0) = -\frac{1}{\sqrt{3}} \cos\theta_\rho$$

$$\rho_f = f_T \rho_i f_T^\dagger = \frac{1}{3} \cos^2\theta_\rho$$

Next, we consider the example ${}^3S_1(p\bar{p}) \to \rho^\pm \pi^\mp$. Here the initial state has $J^{PC} = 1^{--}$, so in order to couple a 1^- and a 0^1 particle to get total $J = 1$, we must have $L = 1$. Similarly, $S_\rho = 1$, $S_\pi = 0$ so $S = 1$. For the transition to $\rho\pi$, we get:

$$\begin{array}{ccccc} T_{10} & & \langle 1+1 \mid 110+1 \rangle \langle 1+1 \mid 10+10 \rangle & & -\frac{1}{\sqrt{2}} \\ T_{00} & = & \langle 10 \mid 1100 \rangle \langle 10 \mid 1000 \rangle & = & 0 \\ T_{-10} & & \langle 1-1 \mid 110-1 \rangle \langle 1-1 \mid 10-10 \rangle & & \frac{1}{\sqrt{2}} \end{array}$$

$$f_{\lambda,0,M} = \begin{pmatrix} -\frac{1}{\sqrt{2}} \mathcal{D}^{*1}_{11}(\phi,\theta,0) & -\frac{1}{\sqrt{2}} \mathcal{D}^{*1}_{01}(\phi,\theta,0) & -\frac{1}{\sqrt{2}} \mathcal{D}^{*1}_{-11}(\phi,\theta,0) \\ 0 & 0 & 0 \\ \frac{1}{\sqrt{2}} \mathcal{D}^{*1}_{1-1}(\phi,\theta,0) & \frac{1}{\sqrt{2}} \mathcal{D}^{*1}_{0-1}(\phi,\theta,0) & \frac{1}{\sqrt{2}} \mathcal{D}^{*1}_{-1-1}(\phi,\theta,0) \end{pmatrix}$$

In this problem, we could have a prefered direction: the spin direction of the initial state. As such, we need to allow for a single angle, θ as measured from the z–axis. However, we can nominally set $\phi = 0$. Under these assumptions, the matrix simplifies to:

$$f_{\lambda,0,M} = \begin{pmatrix} -\frac{1}{\sqrt{2}} d^1_{11}(\theta) & -\frac{1}{\sqrt{2}} d^1_{01}(\theta) & -\frac{1}{\sqrt{2}} d^1_{-11}(\theta) \\ 0 & 0 & 0 \\ \frac{1}{\sqrt{2}} d^1_{1-1}(\theta) & \frac{1}{\sqrt{2}} d^1_{0-1}(\theta) & \frac{1}{\sqrt{2}} d^1_{-1-1}(\theta) \end{pmatrix}$$

The subsequent decay for $\rho \to \pi\pi$ can now be expressed as:

$$f_{0,0M} = \left(\mathcal{D}^{*1}_{10}(\phi_\rho, \theta_\rho, -\phi_\rho),\, \mathcal{D}^{*1}_{00}(\phi_\rho, \theta_\rho, -\phi_\rho),\, \mathcal{D}^{*1}_{-10}(\phi_\rho, \theta_\rho, -\phi_\rho) \right)$$

From these, we can compute the total transition amplitude as a sum over all possible values of ρ helicity, λ_1.

$$f_T = \sum_{\lambda_1} f_{0,0\lambda}(\theta_\rho, \phi_\rho) f_{\lambda_1,0m}(\theta, 0)$$

Performing this sum, we get a vector with elements that correspond to each M component of the initial state.

$$f_T = \left(-\frac{\sin\theta_\rho}{\sqrt{2}} e^{i\phi_\rho}, \cos\theta_\rho, \frac{\sin\theta_\rho}{\sqrt{2}} e^{-i\phi_\rho} \right) \begin{pmatrix} -\frac{1}{\sqrt{2}}\frac{1+\cos\theta}{2} & -\frac{1}{\sqrt{2}}\frac{\sin\theta}{\sqrt{2}} & -\frac{1}{\sqrt{2}}\frac{1-\cos\theta}{2} \\ 0 & 0 & 0 \\ \frac{1}{\sqrt{2}}\frac{1-\cos\theta}{2} & \frac{1}{\sqrt{2}}\frac{-\sin\theta}{\sqrt{2}} & \frac{1}{\sqrt{2}}\frac{1+\cos\theta}{2} \end{pmatrix}$$

Which upon expansion, can be written as:

$$f_T = \left(\frac{1}{\sqrt{2}} \sin\theta_\rho \left[\cos\phi_\rho + i\cos\theta\sin\phi_\rho\right] \; i\sin\theta\sin\theta_\rho\sin\phi_\rho \; \frac{1}{\sqrt{2}}\sin\theta_\rho \left[\cos\phi_\rho - i\cos\theta\sin\phi_\rho\right] \right)$$

Now, to get the final density matrix as followis, and the angular distribution can be obtained by taking the trace of this.

$$\rho_f = f_T \rho_i f_T^\dagger$$
$$w_D = \mathrm{Tr}(\rho_f)$$

A possible initial density matrix is given as follows, where we know that the trace must be equal to 1, or $2a + b = 1$.

$$\rho_i = \begin{pmatrix} a & 0 & 0 \\ 0 & b & 0 \\ 0 & 0 & a \end{pmatrix}$$

If we evaluate this, we find that

$$\rho_f = a\sin^2\theta_\rho \left[\cos^2\phi_\rho + \sin^2\phi_\rho\cos^2\theta\right] + b\sin^2\theta\sin^2\theta_\rho\sin^2\phi_\rho$$
$$w_D = \sin^2\theta_\rho \left[\sin^2\phi_\rho(a\cos^2\theta + b\sin^2\theta) + a\cos^2\phi_\rho\right]$$

In the case where $a = b = \frac{1}{3}$, (unpolarizaed), we find that

$$w_D = \frac{1}{3}\sin^2\theta_\rho$$

5.3 Putting it all together

We have now looked at both resonance shapes, and the angular distributions of all final state particles. We now want to combine these, to produce a total amplitude as given in equation 41. The sum is over all possible transition amplitudes, M, while the product is over all resonance chains within that amplitude, R.

$$w_D = \mathrm{Tr}\left\{ \left[\sum_{k=1}^{M} \left(\gamma_k f_k \prod_{j=1}^{R} \mathcal{BW}_k(j) \right) \right] \rho_i \left[\left(\gamma_k f_k \prod_{j=1}^{R} \mathcal{BW}_k(j) \right) \right]^\dagger \right\} \tag{41}$$

The f_k are the transition amplitudes from above, while the $\mathcal{BW}$ terms parameterize the resonance shape. The γ_k are a priori unknown complex coefficients.

As mentioned earlier, relative decay rates are important, and we need to be able to pull these out of the data. Unfortunately, it is not obvious how we are going to do this with what we currently have. The simple Breit Wigner forms provide no natural mechanism for this. We may also have thresholds that occur in the middle of our resonance. One way to treat this is using a Flatte form [flatte76]. Here the g_i are related to the partial widths in each of two final states, while the ρ_i are the phase space available for each final state.

$$T(\text{mode}_1) = \frac{bg_1}{m_0^2 - m^2 - i(\rho_1 g_1^2 + \rho_2 g_2^2)}$$
$$T(\text{mode}_2) = \frac{bg_2}{m_0^2 - m^2 - i(\rho_1 g_1^2 + \rho_2 g_2^2)}$$
$$\sum g_i^2 = m_0 \Gamma_0$$

$$\rho_1(m) = \frac{2p_1}{m} \qquad \rho_2(m) = \frac{2p_2}{m}$$

Note that at threshold, p_i becomes 0, and ρ_i goes to zero. When we are under threshold, then ρ_i becomes imaginary.

We can actually handle things a bit better by returning to scattering theory, and writing down the transition from some initial state to a final state via an S–Matrix, which in turn can be written as a T–matrix. For a good reference on this, see [chung96].

$$S = I + 2iT$$

The T–matrix describes the transition from the initial to final state, and it can itself be written in terms of a K–matrix, where $K = K^\dagger$.

$$K^{-1} = T^{-1} + iT$$

This can be inverted to yield:

$$T = K(I - iK)^{-1} = (I - iK)^{-1}K.$$

From this, it is possible to get to the familiar form for a resonance,

$$T = e^{i\delta} \sin\delta$$

and

$$K = \tan\delta.$$

If we consider a process where we have several different initial states each with the same quantum numbers, α, and each potentially decaying to many different final states. The states have K–matrix masses m_α, and K–matrix widths Γ'_α. The elements of the n by n K–matrix are given as:

$$K_{ij}(m) = \sum_\alpha \frac{\gamma_{\alpha i}\gamma_{\alpha j} m_\alpha \Gamma'_\alpha}{m_\alpha^2 - m^2} B_{\alpha i}(m) B_{\alpha j}(m) + C_{ij},$$

where the i and j index correspond to decays final states of the states, α. The $\gamma_{\alpha i}$ are real numbers which are the coupling constants for the initial state α to the final state i, such that $\sum_i \gamma_{\alpha i}^2 = 1$. The partial width into some final state i, $\Gamma_{\alpha i} = \gamma_{\alpha i}^2 \Gamma'_\alpha$. The K–matrix total width, $\Gamma_\alpha = \sum_i \Gamma_{\alpha i}$. Finally, there are barrier factors are given as the ratio:

$$B_{\alpha i} = \frac{F_L(p_i)}{F_L(p_{\alpha i})}$$

where $p_{\alpha i}$ is evaluated at the K–matrix mass. This formalism now allows us to account for multiple resonances with the same quantum numbers with multiple decay modes. In the case of one resonance with one decay mode, we can easily transform the K–matrix into a T–matrix:

$$T = \frac{m_0 \Gamma_0 B^2(m)/\rho(m_0)}{m_0^2 - m^2 - i m_0 \Gamma m}$$

where

$$\Gamma(m) = \Gamma_0 \frac{\rho(m)}{\rho(m_0)} B^2(m)$$

What we have at this point describes the decay of an already created resonance. In order to be complete, we need to describe the production of this resonance, through some presumably unknown mechanism. One way to do this is with a P–vector, $P_j(m)$.

$$P_j(m) = \sum_\alpha \frac{\beta_\alpha \gamma_{\alpha j} m_\alpha \Gamma'_\alpha B_{\alpha j}}{m_\alpha^2 - m^2}$$

The β_α are unknown complex production strengths for each K–matrix pole. The production vector can be combined with the subsequent decay to define an F–Vector,

$$\mathcal{F} = (1 - iK\rho)^{-1} P, \tag{42}$$

where the matrix ρ contains the phase space factors, $\rho(m) = 2p_i/m$ along its diagonal, and zero elsewhere. Multiple resonances with multiple decays can now be handled within this prescription. There is one additional complication in that if the daughter products of the resonance subsequently decay as well, then the F–vector in equation 42 is modified by multiplying by the T–matrices of the daughter's decays.

$$\mathcal{F} = \left[(1 - iK\rho)^{-1} P\right] \prod T_j \tag{43}$$

In fitting data with these amplitudes, it is natural to use the K–matrix parameters, m_α and Γ'_α as the fitting parameters. These quantities should not be quoted as the resonance parameters, rather one should use these to determine the T–matrix, and then search for its poles in the complex energy plane.

Depending on how the experiment is performed, it is often possible to decouple the helicity pieces form the resonance parameterization. In these approaches, one uses

the helicity forms to define partial waves, and then fits the data to obtain intensities and phases of these waves as a function of the mass of the system. In a subsequent fit, these first distributions are fit with the resonance parameterizations to extract information on the states themselves. In other experiments, everything must be fit at once. In both of these cases, understanding the acceptance of the detector system and having good detector resolution is crucial. In fact, the closer the acceptance is to perfect, the better the measurement will be. It is key in designing detectors for this type of physics that as uniform an acceptance as possible be built into the highest resolution system possible.

6 Overview of The Current Data

I now want to proceed with data a results from a number of recent and current experiments. These experiments provide the best evident to date that we have seen observed gluonic excitations.

6.1 The Status of Glueballs

As discussed in section 4.1, the lightest glueball is expected to be a scalar state, $\mathbf{J^{PC}} = 0^{++}$ with a mass in the range of 1.5 to 1.7 GeV/c^2. In addition, we want to look for this in so called *glue–rich* reactions, such as J/ψ decays, $p\bar{p}$ annihilation, and central production.

6.1.1 $\bar{p}p$ Annihilations at Rest

The most significant data on $\bar{p}p$ annihilations has come from the Crystal Barrel experiment running at the Low Energy Antiproton Ring at CERN [aker92]. This experiment has collected a huge statistics of data on $p\bar{p}$ annihilations both at rest and in flight. A very good review of this experiment can be found in [amsler98]. Here we wish to concentrate on a small subset of that experiment's results.

In particular, the reactions $p\bar{p}$ at rest goes to $\pi^\circ\pi^\circ\pi^\circ$, $\pi^\circ\eta\eta$, $\pi^\circ\eta\eta'$ and $\pi^\circ K_L K_L$. All of these final states could be formed via the reaction:

$$p\bar{p} \to \pi^\circ X \to \pi^\circ M_1 M_2.$$

in addition, the two identical pseudoscalar mesons can combine to make $(\mathbf{I^G})\mathbf{J^{PC}} = (0^+)0^{++}$ and $(0^+)2^{++}$, or f_0 and f_2 states. Of course there can and will be other things in these data by pairing up other mesons, but the key point is that we can look for f_0 states decaying to many different final states.

The data in these analyses are presented in the form of a Dalitz plot. A three body system from an unpolarized initial state at rest, the final state can be uniquely described by two variables. One possible choice is any pair of invariant masses squared. For the reaction $X \to a + b + c$, there are three possible two–invariant masses, m^2_{ab}, m^2_{bc} and m^2_{ac}. These are actually related to each other via

$$m_x^2 + m_a^2 + m_b^2 + m_c^2 = m_{ab}^2 + m_{bc}^2 + m_{ac}^2$$

In Fig. 18 are shown the Dalitz plots for $p\bar{p}$ annihilation at rest into $\pi^\circ\pi^\circ\pi^\circ$ and $\pi^\circ\eta\eta$. While the analyses of these channels involve many intermediate resonances [amsler95a, amsler95c], there is one new state which stands out in both, the $f_0(1500)$. This state has a mass of $1505\,\mathrm{MeV/c^2}$ and a width of $110\,\mathrm{MeV/c^2}$. In later analysis [amsler95b, amsler94a], the $f_0(1500)$ has also been observed in the $\eta\eta'$ and K_LK_L final states, (see Fig. 19). Examining all these data, it is possible to extract many different annihilation–decay rates for the $f_0(1500)$ as given in table 11. If we recall equation 19 from section 3, we can convert the numbers in this table into relative decay amplitudes squared, γ^2, which if normalized to the $\eta\eta$ mode are given in table 12.

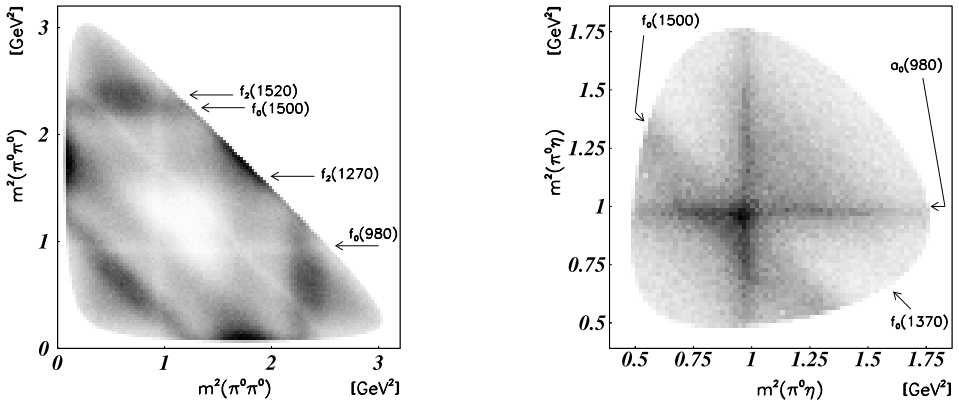

Figure 18: Dalitz plots for $\bar{p}p$ annihilation into three pseudoscalar mesons. The left is $\pi^\circ\pi^\circ\pi^\circ$, and the right is $\pi^\circ\eta\eta$.

Decay	*Rate*	$q\,[\mathrm{GeV/c}]$
$f_0(1500) \to \pi\pi$	0.290 ± 0.075	0.740
$f_0(1500) \to K\bar{K}$	0.035 ± 0.003	0.567
$f_0(1500) \to \eta\eta$	0.046 ± 0.013	0.516
$f_0(1500) \to \eta\eta'$	0.012 ± 0.003	0.0889
$f_0(1500) \to 4\pi$	0.617 ± 0.096	0.5

Table 11: Measured branching fractions for $\bar{p}p \to f_0(1500)\pi^\circ$.

The rates in table 12 can now be compared to the SU(3) predictions given in Fig. 2 to see if the $f_0(1500)$ can be identified as a normal meson. In Fig 20 are plotted both the Crystal Barrel data and the relative rates as computed from SU(3) for an f_0' as

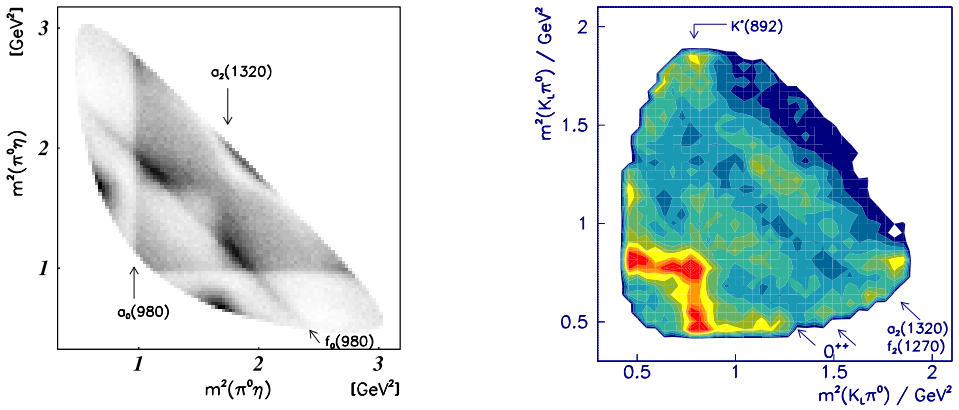

Figure 19: Dalitz Plots for $\bar{p}p$ annihilation into three pseudoscalar mesons. The left is $\pi^\circ K_L K_L$and the right is $\pi^\circ\eta\eta'$.

a function of the nonet mixing angle. While a normal meson with a mixing angle of about 143° can accommodate the $K\bar{K}$, $\eta\eta$ and $\eta\eta'$ modes, it is a factor of ~ 4 too small with respect to the observed $\pi\pi$ modes. There is a bit of controvery about how the $\pi\pi$ is calculated, the 2002 edition of the Particle Data Book [pdg02] actually lists a larger number. In fact, 143° corresponds to a mostly $u\bar{u}$ and $d\bar{d}$ state, not and $s\bar{s}$ state.

$$f(\theta = 143^\circ) = 0.91\bar{n}n + 0.09\bar{s}s \tag{44}$$

The best comparison for a meson is shown in table 12, and at least in this model, it is looks like the $f_0(1500)$ is not a normal meson. One can also compare to the decay rates of a pure glueball, and again it is clear that the $f_0(1500)$ is not a pure glueball. At this point, it's exact nature is unclear, but if it is a pure $q\bar{q}$ state, it is mostly $u\bar{u}anddd\bar{}$.

Decay Rate	$\pi\pi$	$\bar{K}K$	$\eta\eta$	$\eta\eta'$	4π
$f_0(1500)$	5.13 ± 1.95	0.708 ± 0.209	1.00	1.64 ± 0.62	13.7 ± 4.4
Meson	14	1.4	1	2.4	
Glueball	3	4	1	0	Large

Table 12: Relative decay amplitudes squared, γ^2 normalized to the $\eta\eta$ rate for the $f_0(1500)$. These are compared to the SU(3) prediction for an $s\bar{s}$ meson with mixing angle of 150°, as well as for a pure glueball.

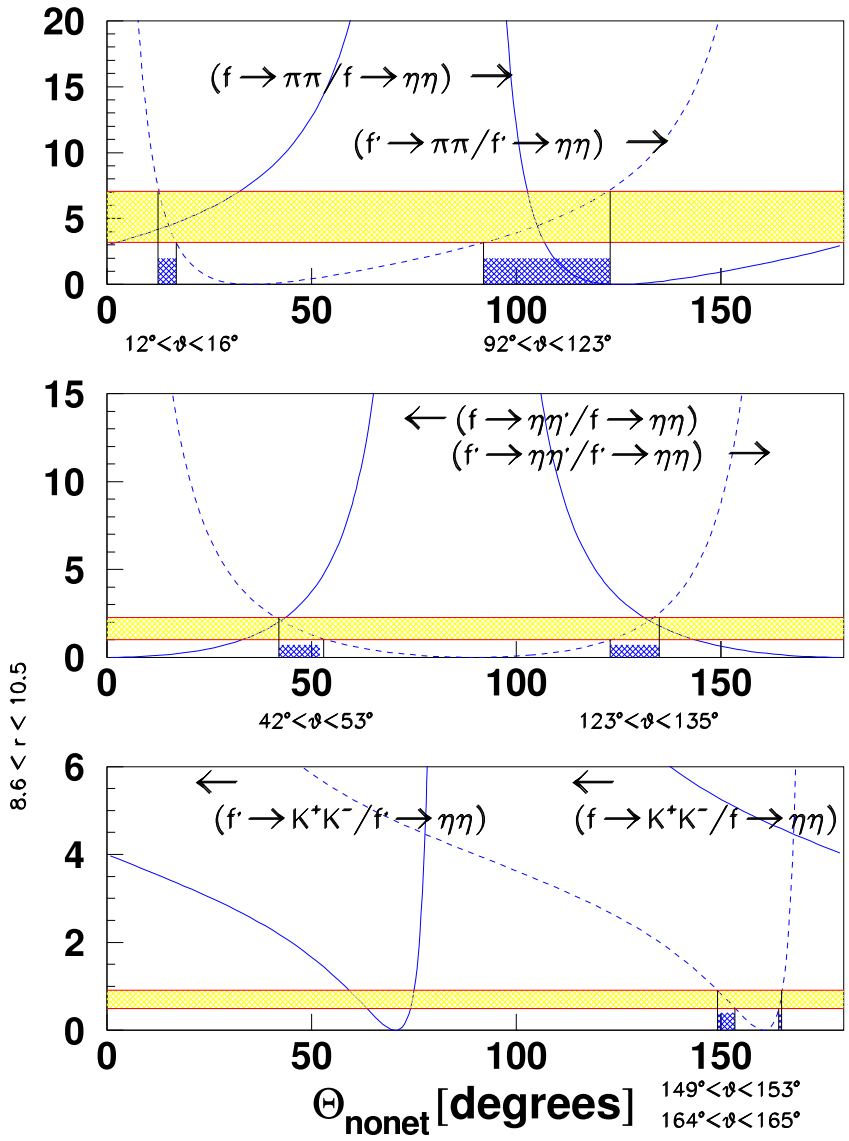

Figure 20: The experimental decay rates of the $f_0(1500)$ compared to the SU(3) predictions for an f_0 and f_0' state decaying into pairs of pseudoscalar mesons as a function of the scalar nonet mixing angle. There is no angle which is consistent with the measured data.

6.1.2 Central Production Experiments

Another glue-rich channel is that of central production, and a great deal of analysis has been done recently by the WA102 collaboration at CERN. WA102 have looked at central production of $\pi^+\pi^-$ [barberis95, barberis99b], $\pi^\circ\pi^\circ$ [barberis99c], $K\bar{K}$ [barberis99a], and $\pi^+\pi^-\pi^+\pi^-$ [barberis95, barberis97b] in 450 GeV/c pp collisions. In all of these analyses, they observe two scalar states, the $f_0(1500)$ and the $f_0(1710)$. In addition, in the 4π data, they observe the $f_0(1370)$. They also find that by kinematically selecting on their data, they were able to enhance the scalar signals.

State	Mass GeV/c^2	Width GeV/c^2	Decay	Reference
$f_0(980)$	0.985 ± 0.010	0.065 ± 0.020	K^+K^-	[barberis99a]
$f_0(980)$	0.982 ± 0.003	0.080 ± 0.010	$\pi^+\pi^-$	[barberis99b]
$f_0(1370)$	1.290 ± 0.015	0.290 ± 0.030	$\pi^+\pi^-\pi^+\pi^-$	[barberis97b]
$f_0(1370)$	1.308 ± 0.010	0.222 ± 0.020	$\pi^+\pi^-$	[barberis99b]
$f_0(1500)$	1.502 ± 0.010	0.131 ± 0.015	$\pi^+\pi^-$	[barberis99b]
$f_0(1500)$	1.497 ± 0.010	0.104 ± 0.025	K^+K^-	[barberis99a]
$f_0(1500)$	1.510 ± 0.020	0.120 ± 0.035	$\pi^+\pi^-\pi^+\pi^-$	[barberis97b]
$f_0(1710)$	1.700 ± 0.015	0.100 ± 0.025	K^+K^-	[barberis99a]
$f_0(2000)$	2.020 ± 0.035	0.410 ± 0.050	$\pi^+\pi^-\pi^+\pi^-$	[barberis97b]

Table 13: Observed scalar mesons in various final states in WA102.

In Fig. 10a, the quantities q_1 and q_2 represent the four–momentum transfer from each proton to the produced system, X. WA102 observed a striking difference between ratio of events with $\mid \vec{q_1} - \vec{q_2} \mid$ small as compared to those with this quantity large. Events with exotic candidates such as the $f_0(1500)$ and $f_J(1710)$ had large ratios, while events with normal mesons had small ratios for this quantity [barberis96, barberis97a].

State	Mass GeV/c^2	Width GeV/c^2
$f_0(980)$	$0.987 \pm 6 \pm 6$	$0.096 \pm 0.024 \pm 0.016$
$f_0(1370)$	$1.312 \pm 25 \pm 10$	$0.218 \pm 0.044 \pm 0.030$
$f_0(1500)$	$1.502 \pm 12 \pm 10$	$0.098 \pm 0.018 \pm 0.016$
$f_0(1710)$	$1.727 \pm 12 \pm 11$	$0.126 \pm 0.016 \pm 0.018$

Table 14: T–Matrix pole positions from a WA102 coupled channel analysis [barberis99d].

A recent analysis by WA102 [barberis99d] has performed a coupled channel analysis of the $\pi^+\pi^-$ and K^+K^- systems. This analysis using both T–matrix and K–matrix forms finds four poles, meaning that four scalar states are needed to describe the data. These states are given in table 14. Recently a compilation of many of these ratios as measured in WA102 has appeared [close01]. These relative decay rates for all three scalar states are given in Table 15. Repeating the same simple SU(3) analysis that was performed with the Crystal Barrel data. The results are shown in Table 16.

State	$f_0(1370)$	$f_0(1500)$	$f_0(1710)$
$K\bar{K}$:$\pi\pi$	0.467 ± 0.194	0.32 ± 0.07	5.0 ± 0.75
$\eta\eta$:$K\bar{K}$	0.35 ± 0.21		0.48 ± 0.14
$\pi\pi$:$\eta\eta$		5.5 ± 0.84	
$\eta\eta'$:$\eta\eta$		0.52 ± 0.16	$< 0.05(90\%CL)$

Table 15: Measured relative decay rates as taken from the WA102 experiment at CERN. These results are taken from a summary by Close and Kirk [close01]. Isospin corrections have been performed.

What is interesting is that the best solution for is around 112°, which corresponds to a mostly $u\bar{u}$ and $d\bar{d}$ state. The solution around 0° corresponds to the $f_0(1370)$ being a nearly perfect octet state. In the case of the $f_0(1500)$, the solution is not great, but is consistent with the Crystal Barrel picture of the state being mostly $u\bar{u}$ and $d\bar{d}$. In fact, if the angle were 120°, it would be a purely $n\bar{n}$ state. The $f_0(1710)$ has a very poor fit as a simple $q\bar{q}$ system, but if it were forced to be pure system, the best mixing angle is around 90°, which would make it a nearly pure SU(3) singlet state.

Particle	θ	χ^2	θ	χ^2
$f_0(1370)$	$112° \pm 12°$	0.1	$2° \pm 1°$	2.2
$f_0(1500)$	$118° \pm 3°$	14		
$f_0(1710)$	$87° \pm 2°$	23		

Table 16:

6.1.3 Radiative J/ψ Decays

In radiative J/ψ decays, the results are hampered by the finite statistics that have been collected to date. There are plans to increase the sample from the BES detector to about 20×106 by 2001, but even this increase by a factor of 3 over current samples is still going to leave things ambiguous. There are reports of all three f_0 states in these decays, as given in table 17. However, there are some inconsistencies. Both [bai96] and [bugg95] find both a 0^{++} and a 2^{++} signal near 1.7GeV/c^2. However, [dunwoodie97] finds only a 0^{++} signal. In addition, [dunwoodie97] sees the $f_0(1370)$ in radiative J/ψ decays, while [bai96] and [bugg95] do not. Finally, both [bugg95] and [bai96] see the $f_0(1500)$, while [dunwoodie97] does not.

6.1.4 Other Data

6.1.5 Interpretation

If we examine the scalar data as a whole, there appears to be three states, $f_0(1370)$, $f_0(1500)$ and $f_0(1710)$. The decay pattern of the $f_0(1500)$ seem to exclude it being simply a meson. In addition, its strong production in $\bar{p}p$ annihilation at rest seem to

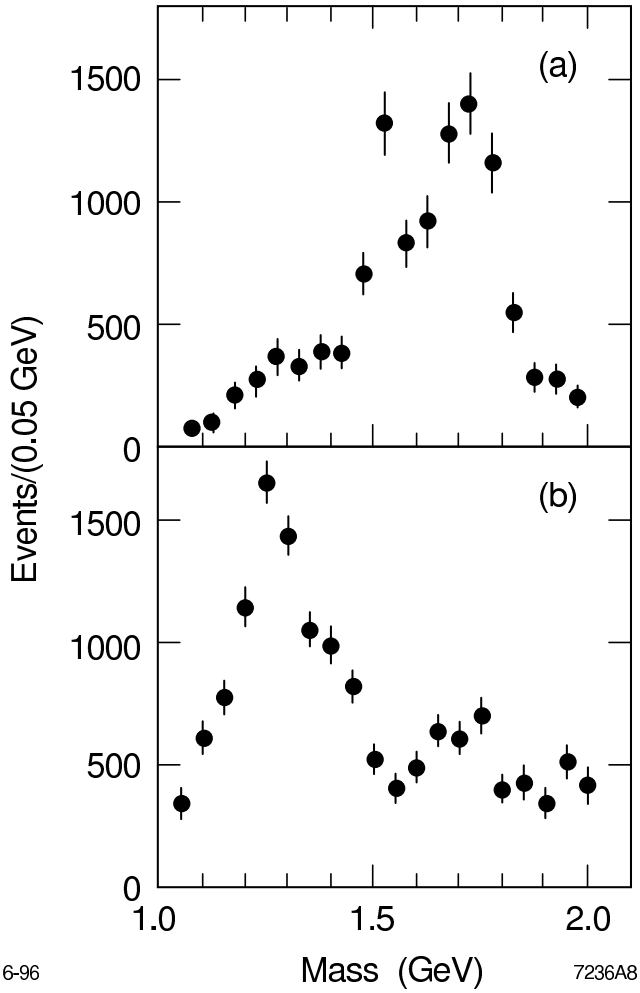

Figure 21: Data taken from the Mark III experiment. These have been acceptance and isospin corrected. (**a**) Events from $J/\psi \to \gamma(K^+K^-)$, (**b**) Events from $J/\psi \to \gamma(\pi^+\pi^-)$.

State	Mass GeV/c^2	Width GeV/c^2	Decay	Rate (10^{-4})	Reference
$f_0(1370)$	$1.429^{+0.043}_{-0.037}$	$0.169^{+0.111}_{-0.076}$	$\pi\pi$	$(3.7^{+2.3}_{-1.5})$	[dunwoodie97]
$f_0(1370)$	$1.429^{+0.043}_{-0.037}$	$0.169^{+0.111}_{-0.076}$	$K\bar{K}$	$(0.6^{+0.4}_{-0.2})$	[dunwoodie97]
$f_0(1500)$	$1.505^{\dagger}$	$0.120^{\dagger}$	$\pi^+\pi^-\pi^+\pi^-$	(2.5 ± 0.4)	[bugg95]
$f_0(1710)$	$1.704^{+0.016}_{-0.023}$	$0.124^{+0.052}_{-0.044}$	$\pi\pi$	$(2.0^{+0.5}_{-0.4})$	[dunwoodie97]
$f_0(1710)$	$1.704^{+0.016}_{-0.023}$	$0.124^{+0.052}_{-0.044}$	$K\bar{K}$	$(7.5^{+2.0}_{-1.6})$	[dunwoodie97]
$f_0(1710)$	$1.781^{+0.018}_{-0.039}$	$0.085^{+0.046}_{-0.043}$	K^+K^-	$(0.8^{+0.4}_{-0.2})$	[bai96]
$f_0(1710)$	1.750 ± 0.015	0.160 ± 0.040	$\pi^+\pi^-\pi^+\pi^-$	(4.3 ± 0.6)	[bugg95]

Table 17: Observed signals for $J/\psi \to \gamma f_0$

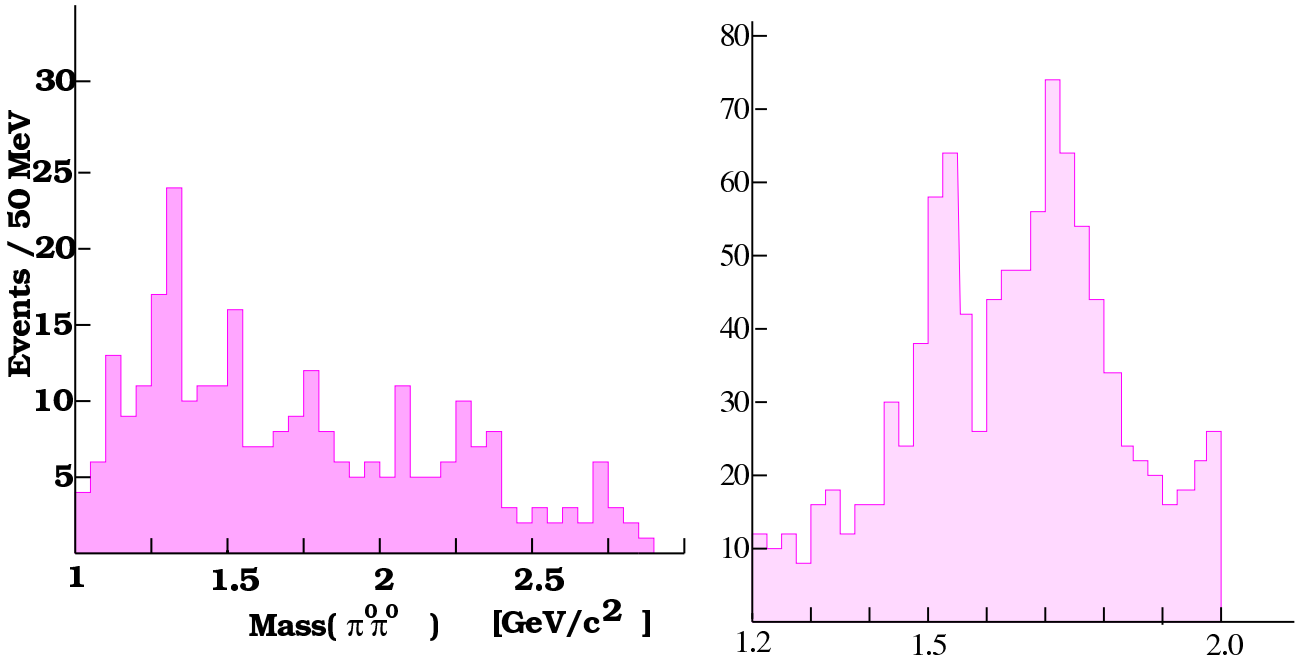

Figure 22: Data taken from the BES experiment. (**a**)Events from $J/\psi \to \gamma(\pi^+\pi^-)$ (**b**) Events from $J/\psi \to \gamma(K^+K^-)$.

State	$f_0(1370)$	$f_0(1710)$
$K\bar{K}$:$\pi\pi$	$0.149 + 0.215 - 0.133$	$3.73 + 1.67 - 2.35$

Table 18: Relative $K\bar{K}$ to $\pi\pi$ decay rates from Mark III [dunwoodie97]. Isospin corrections have been performed.

exclude it being a mostly $s\bar{s}$ state. All three states are observed in central production, while the $f_0(1710)$ is clearly observed in J/Ψ decays, with some conflicting information on the other two states. The simplest explanation of what we observe appears to be that the two scalar mesons, f_0 and f_0' along with the scalar glueball exist, and that they have mixed to form the three observed states, $f_0(1370)$, $f_0(1500)$ and $f_0(1710)$.

In order to try and understand this picture, we will extend the earlier mixing picture to allow the glueball to mix with the isoscalar states. To do this, we need to define two additional mixing angles, which for convenience we will call α and ξ. We also need to allow for a strength of the glueball decay to mesons that may be different from the meson decay, R. In this scheme, we can use the summary in table 7 to write the three observed states in terms of the three SU(3) basis states as follows:

$$\begin{bmatrix} f \\ f' \\ f'' \end{bmatrix} = \begin{pmatrix} \cos\xi\cos\theta\cos\alpha - \sin\alpha\sin\xi & \cos\xi\sin\theta & \cos\xi\cos\theta\sin\alpha + \sin\xi\cos\alpha \\ -\sin\theta\cos\alpha & \cos\theta & -\sin\theta\sin\alpha \\ -\sin\xi\cos\theta\cos\alpha - \cos\xi\sin\alpha & -\sin\xi\sin\theta & \cos\alpha\cos\xi - \sin\xi\cos\theta\sin\alpha \end{pmatrix} \begin{bmatrix} |\,1\rangle \\ |\,8\rangle \\ |\,\mathcal{G}\rangle \end{bmatrix}$$

In this scheme, if the angles ξ and α are zero, we reduce to $f = \cos\theta|1> + \sin\theta|8>$ and $f' = -\sin\theta|1> + \cos\theta|8>$, the standard nonet mixing scheme. In computing

the decay ratios, we need to remember to scale the decay of the gluons by a factor of R. It is also convenient to rewrite the SU(3) states in terms of their light quark, $n\bar{n}$ and strange quark, $s\bar{s}$ content. Most of the following will express the mixing in terms of these states, while the decays are computed in terms of the SU(3) states.

$$\begin{aligned} |\,1\rangle &= \sqrt{\frac{2}{3}}\left(\frac{u\bar{u}+d\bar{d}}{\sqrt{2}}\right)+\sqrt{\frac{1}{3}}s\bar{s} \\ &= \sqrt{\frac{2}{3}}n\bar{n}+\sqrt{\frac{1}{3}}s\bar{s} \\ |\,8\rangle &= \sqrt{\frac{1}{3}}\left(\frac{u\bar{u}+d\bar{d}}{\sqrt{2}}\right)-\sqrt{\frac{2}{3}}s\bar{s} \\ &= \sqrt{\frac{1}{3}}n\bar{n}-\sqrt{\frac{2}{3}}s\bar{s} \end{aligned}$$

In addition to the three mixing angles, simple SU(3) makes no prediction on the relative decay rate of the glueball with respect to the normal mesons, (g_1^g versus g_T of section 4.1). We can now take all the data on scalar meson decays, and try to fit it to obtain θ, α, ξ and R. If we do so, we find three different solutions as given in table 19. It should be noted that there are several mathematical ambiguities in the the formulation we have written down. It is fairly strait forward to show that without loss of generality, we can restrict R to be negative, and the three mixing angles to be in the range of 0 to π. All solutions outside this range are mathematically equivalent to ones inside the range.

Solution	Ratio	θ	α	ξ	χ^2
a	$-4\sqrt{\frac{2}{5}}$	81.5°	154.5°	133.5°	1.32
b	$-4\sqrt{\frac{2}{5}}$	103.5°	128.5°	132.5°	1.29
c	$-\frac{1}{4}\sqrt{\frac{5}{2}}$	88.5°	100.5°	110.5°	2.04

Table 19: The three minima to the fit of branching ratio data.

Fig. 23a shows a plot of χ^2 against the ratio R. Even though there is a clear minimum around $-4\sqrt{\frac{2}{5}}$, in fact all the values that fall below the 65% line are within one σ errors. It is particularly tricky fitting the angles with only these data. Also, around the deepest minimum, there are actually two distinct solutions as given as **a** and **b** in table 19. However, there is also a second minimum dip around $-\frac{1}{4}\sqrt{\frac{5}{2}}$ as given as **c** in the table. A particular solution can be represented as a fraction of $n\bar{n}$, $s\bar{s}$ and $\mathcal{G}$ in each of the three physical states, $f_0(1370)$, $f_0(1500)$ and $f_0(1710)$. These are represented for the three solutions in Fig. 24. It is clear that even though we cannot pin down the exact mixtures, there are a few common features. First, the $f_0(1500)$ has at most about 30% $s\bar{s}$, and is best described as either largely $n\bar{n}$ or $\mathcal{G}$. The current data favor a large $s\bar{s}$ component and a small $n\bar{n}$ component in the $f_J(1710)$. Finally, it is difficult to say where the $\mathcal{G}$ state is.

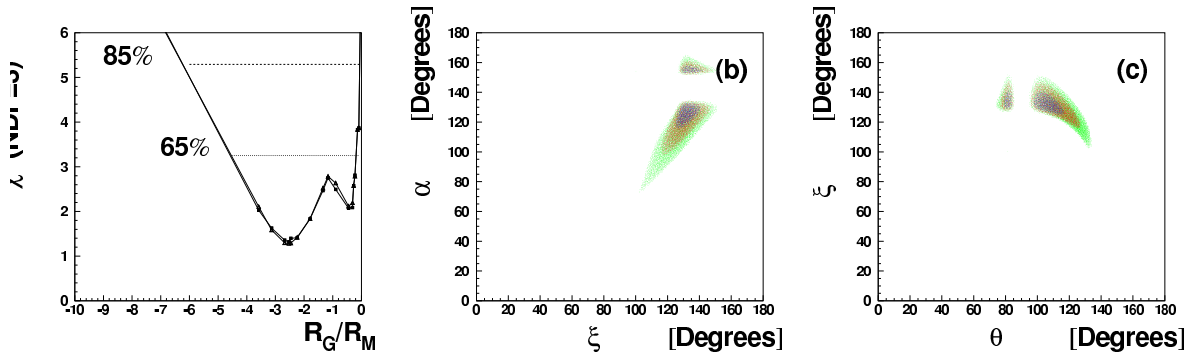

Figure 23: (**a**) shows χ^2 of the fit as a function of the Relative decay strength of the glueball to mesons in the SU(3) picture. The two lines indicate the 65% confidence level and 85% confidence level curves. (**b**) shows a plot of α versus ξ for all solutions that have, 91%, 85% and 65% confidence level. (**c**) shows ξ versus θ for all solutions that have 91%, 85% and 65% confidence level.

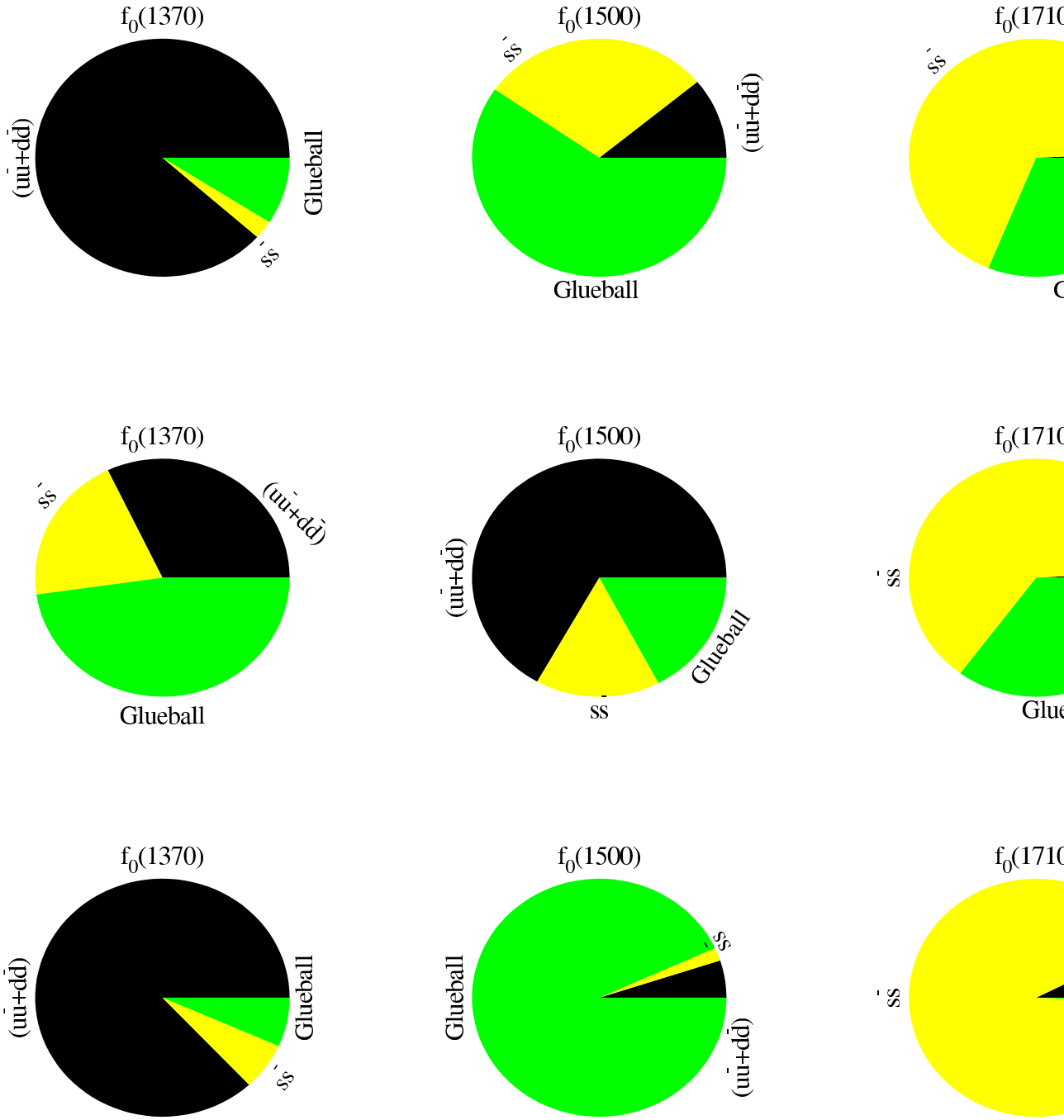

Figure 24: Row 1 is solution **a**, row 2 is solution **b**, and row 3 is solution **c**. The three solutions are from from table 19.

6.2 The Status of Hybrids

The most striking evidence of a hybrid meson would the observation of states with non-$q\bar{q}$ quantum numbers, *e.g.* 0^{--}, 0^{+-}, 1^{-+}, 2^{+-}, $\cdots$. However, this observation by itself would not be sufficient. There are models of $q\bar{q}q\bar{q}$ states which can also have exotic quantum numbers. Such an observation would unequivocally indicate something beyond the normal $q\bar{q}$ structure of mesons.

6.2.1 πp Peripheral production

Brookhaven experiment E852 has reported the observation of two states with 1^{-+} quantum numbers. The first has been observed in the reaction $\pi^- p \to \eta\pi^- p$ [thompson97, chung99]. A partial wave analysis of the $\eta\pi$ system shows evidence of a $J^{PC} = 1^{-+}$ state at a mass of $(1.370 \pm 0.016 + 0.050 - 0.030)\,\mathrm{GeV/c^2}$ and a width of $(0.385 \pm 0.040 + 0.065 - 0.105$ The final state is dominated by the production of the $J^{PC} = 2^{++}$, $a_2(1320)$ and the exotic state is seen mainly through its interference with the a_2. Figure 25 shows the partial wave results of this analysis. The $a_2(1320)$ is seen to dominate the 2^{++} wave as shown in **a**. The other allowed wave is the 1^{-+} exotic wave as shown in **b**. While there does appear to be a peak in this wave, the real evidence for resonant behavior comes from the phase difference between the two waves, (**c**). The lines on top of the data are the best fit. The three contributions to the phase difference are shown in **d** where 4 is the fit phase difference from **c**. 1 is the Breit–Wigner contribution from an a_2 resonance, 2 is the contribution from the exotic wave, and 3 shows the assumed flat background phase. It is under this latter reasonable assumption that two interfering Breit–Wigners give a very good description of the data. This leads to the conclusion that there is a 1^{-+} resonant state. It should be noted that the peak of the exotic wave contains about 400 counts, while the peak of the a_2 contains about 13,000 events. The exotic signal is on the order of 1% of the dominant signal, and it is only through its interference is it extracted. A earlier analysis was performed by the VES collaboration [beladidze93] on the same reaction at different incident π^- energy. They see exactly the same intensity and phase distributions as E852, but due to more limited statistics, did not claim the presence of an exotic signal.

A second analysis by E852 examines $\pi^- p \to \pi^+\pi^-\pi^- p$ [adams98]. The three–pion system is much richer than the $\eta\pi$ system seen before. In particular, $\pi\pi$ pairs could form $(\pi\pi)_s$, $\rho(770)$ or $f_2(1270)$ intermediate states. In fact, due to the presence of non resonant effects at low energy, this analysis is not able to completely understand the data in the $1.4\,\mathrm{GeV/c^2}$ region. However, the $1.6\,\mathrm{GeV/c^2}$ region is dominated by two partial waves. The $\pi_2(1670)$ in the 2^{-+} wave, and a second isospin 1, 1^{-+} exotic state at $m = (1.593 \pm 0.008 + 0.029 - 0.047)\,\mathrm{GeV/c^2}$ and $\Gamma = (0.168 \pm 0.020 + 0.150 - 0.012)\,\mathrm{GeV/c^2}$. Fig. 26 shows plots of the the intensity of these two waves in **a** and **b**, and their phase difference in **c**. In **d** is shown the individual phase motion of these two waves under the Breit–Wigner assumption, and the relative production phase between them.

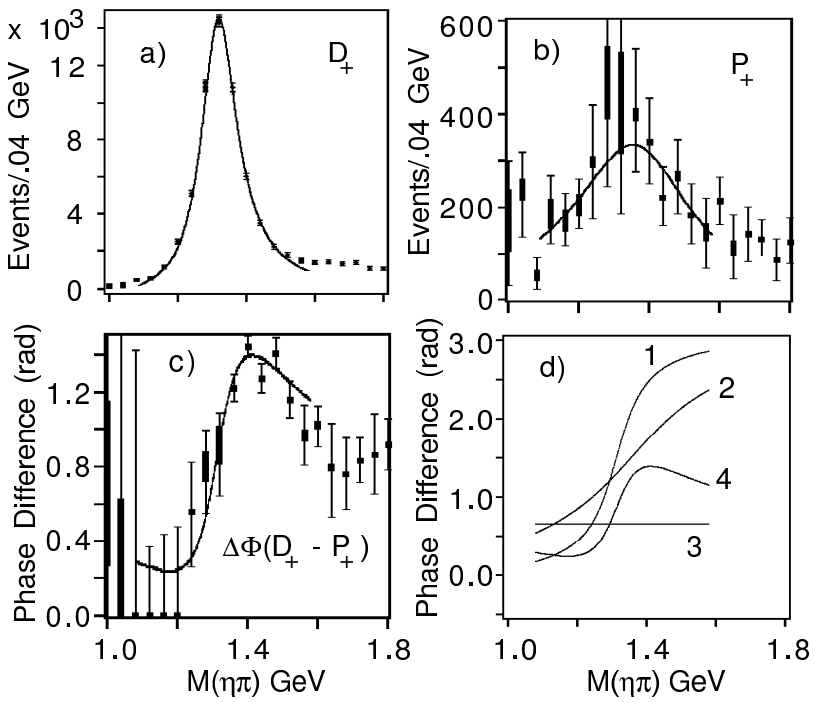

Figure 25: Results from E852 on the partial wave analysis of $\pi^- p \to \eta\pi^- p$. Plot **a** shows the intensity of the 2^{++} wave as a function of mass. Plot **b** shows the intensity of the exotic wave as a function of mass. Plot **c** shows the phase difference between **a** and **b** and **d** correspond to the different elements in the fit to the phase differences.

6.2.2 $p\bar{p}$ Annihilations

The Crystal Barrel experiment has studied the reaction $\bar{p}d \to \pi^-\pi^\circ\eta p$ [abele98] and $\bar{p}p \to \pi^\circ\pi^\circ\eta$ [abele98]. The deuterium annihilation shows the most striking evidence for an exotic 1^{-+} state decaying to $\eta\pi$. The observed mass is $m = (1.400 \pm 0.020 \pm 0.020)\,\mathrm{GeV/c^2}$ and width of $\Gamma = (0.310 \pm 0.050 + 0.050 - 0.030)\,\mathrm{GeV/c^2}$. Annihilation on the neutron has a different set of allowed initial states than from the proton. Table 20 gives the annihilation rates into the possible final states. The $(\eta\pi)_P$ entry corresponds to the 1^{-+} $\eta\pi$ system. What is interesting is that the exotic state is produced nearly as strongly as the $a_2(1320)$ from both allowed initial states. This is unlike the peripheral production where it is on order 1% of the $a_2(1320)$. Secondly, there is a crossing $\rho(770)$ band which provides far more complicated interference. Fig. 27a shows the Dalitz plot for this final state. When this is fit with all final states except the exotic wave, the $\chi^2/\mathrm{ndf} = 1233/(411-12) = 3.07$. Addition of the exotic wave to the fit mixture reduces this $\chi^2/\mathrm{ndf} = 506/(411-20) = 1.29$. It is clear that the exotic wave is a critical component in explaining these data, even though it is not directly visible in the Dalitz plot. Fig. 27b shows where both the intensity and the interference terms from the 1^{-+} wave contribute to the Dalitz plot. The phase motion of the exotic wave is clearly necessary because of both the interference with both the $a_2(1320)$, and the

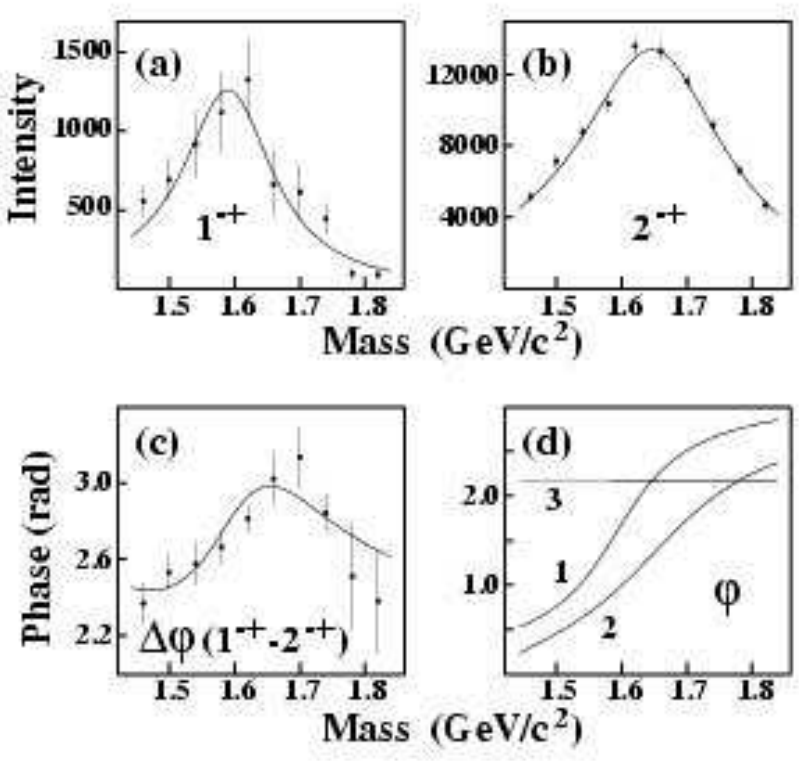

Figure 26: Results from E852 on the partial wave analysis of $\pi^- p \to \pi^+\pi^-\pi^- p$. Plot **a** shows the intensity of the exotic 1^{-+} wave. Plot **b** shows the intensity of the 2^{-+} wave as a function of mass. Plot **c** shows the phase difference between **a** and **b** and **d** correspond to the different elements in the fit to the phase differences.

crossing $\rho^-(770)$.

Initial State	Intermediate State	Rate (%)	Production Phase
$^3S_1(66.4\%)$	$\rho^-(770)\eta$	30.0 ± 3.5	0 (fixed)
$(I^G)J^{PC} = (1^+)1^{--}$	$a_2(1320)\pi$	11.1 ± 1.0	$(7 \pm 8)^\circ$
	$(\eta\pi)_P\pi$	7.9 ± 1.0	$(210 \pm 10)^\circ$
$^1P_1(33.6\%)$	$\rho^-(770)\eta(L=0)$	10.3 ± 3.0	0 (fixed)
$(I^G)J^{PC} = (1^+)1^{+-}$	$\rho^-(770)\eta(L=2)$	17.3 ± 1.2	$(145 \pm 10)^\circ$
	$a_2(1320)\pi$	3.8 ± 0.8	$(315 \pm 25)^\circ$
	$(\eta\pi)_P\pi(L=0)$	2.8 ± 1.3	$(70 \pm 35)^\circ$
	$(\eta\pi)_P\pi(L=2)$	0.5 ± 0.5	$(110 \pm 50)^\circ$

Table 20: Crystal Barrel results on the reaction $\bar{p}d \to \eta\pi^-\pi^\circ$ showing the contribution from each intermediate state to the total reaction. It is interesting to note that the exotic $\eta\pi$–P wave is of similar strength to the $a_2(1320)$ in both initial states.

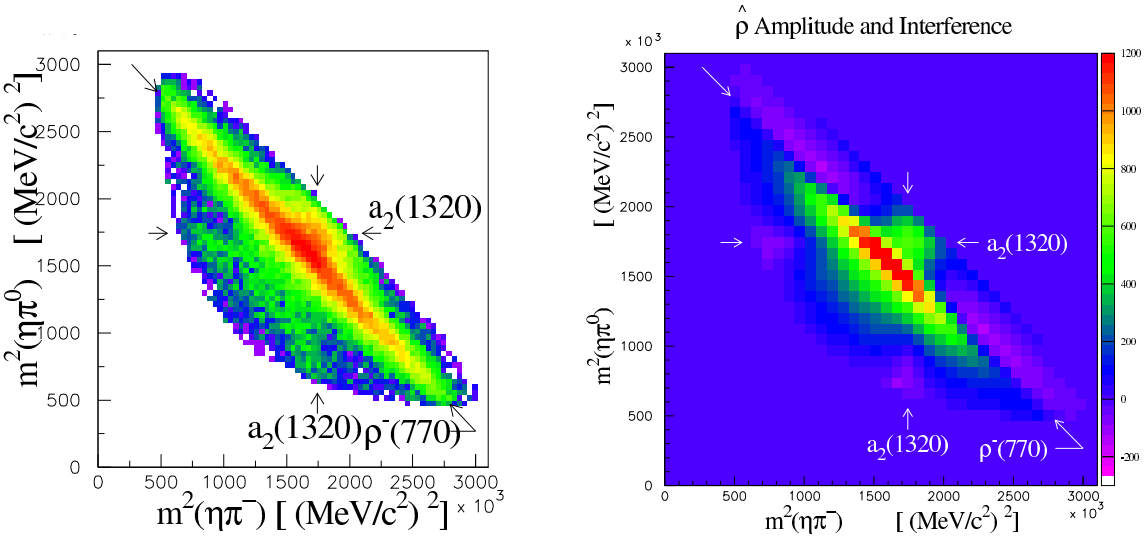

Figure 27: Results from Crystal Barrel on the reaction $\bar{p}d \to \eta\pi^\circ\pi^- p$. **a**:The Dalitz plot for the reaction $\bar{p}n \to \eta\pi^-\pi^\circ$. The dominant diagonal band is the $\rho^-(770)$. One can also see a vertical and horizontal band for the $a_2(1320)$. **b**: The contribution of the exotic $\pi\eta$ wave to the Dalitz plot. While this is not directly observable in the Dalitz plot, its interference with both the a_2 and the ρ are critical in explaining the data.

6.2.3 Interpretation

The obvious question is *Have we found hybrid mesons?* The data seem to indicate two $I = 1$, $J^{PC} = 1^{-+}$ states. One near $m = (1.4)\mathrm{GeV/c^2}$ with a width of about $\Gamma = (0.3)\ \mathrm{GeV/c^2}$, and a second near $m = (1.6)\ \mathrm{GeV/c^2}$ with a width of $\Gamma = (0.17)\ \mathrm{GeV/c^2}$. Neither of these states has been observed in decay modes favored by hybrid mesons. The lighter state is seen in $\eta\pi$, while the heavier one is seen in $\rho\pi$. Both states are lighter than the expected lowest hybrid mass of around $m = (1.8)\ \mathrm{GeV/c^2}$. Finally, only one ($I = 1$) state with these quantum numbers is expected, though we do expect two additional $I = 0$ states, and the corresponding strange states to fill out a nonet of hybrids. It is possible to explain the E852 data on the lower mass state as a threshold effect from the higher mass state interfering with a background precess that is typical in pion production [donnachie98]. However, this explanation fails for the Crystal Barrel result. In order for it to work here, there would have to be a different background in $\bar{p}p$ annihilation that conspired in exactly the same way to produce exactly the same signal. This seems highly unlikely, and relies on the statistically more significant Crystal Barrel results being wrong. Other explanations with threshold effects have also been proposed most relying on the fact that both the $f_1(1285)\pi$ and $b_1(1235)\pi$ thresholds are near the observed mass of 1.4. Actually, a better understanding of this state will only come from studies of the $f_1(1285)\pi$ and $b_1(1235)\pi$ final states.

The $1.6\,\mathrm{GeV/c^2}$ state is closer in mass to the expected hybrids, but again, its decay to $\rho\pi$ is not expected to be a large hybrid decay mode. Additional information is needed on different decay modes of this state. Also, to demonstrate that a hybrid meson has been seen, it is important to find more than one member of the nonet. Currently, an $I = 1$ object has been seen, but we expect two $I = 0$ objects as well.

7 The Future of Spectroscopy

So given where we stand, what is the future of light quark spectroscopy? Over the last few years we have seen tremendous advances in theory, and with the current rate of improvements, we can only expect this to continue. We have also seen the first hard evidence of non–$q\bar{q}$ states with exotic quantum numbers, and there is good evidence that that ground state glueball has been found, but that it is mixed into three states. In order to see what it next, we would like to look at Fig. 15, and focus in on the mass region of $1.5\,\mathrm{to}\,2.5\,\mathrm{GeV/c^2}$. This region encompasses the lowest lying hybrid nonets and glue ball states. It unfortunately also covers several orbital and radial excitations of $q\bar{q}$ states. Identifying and untangling the nature of the states in this region is key in fully understanding the bound states of QCD. There are several areas where progress could be made and one in particular where almost no data exist. This latter case is the photoproduction of mesons. Due mostly to beam intensity limits, typical earlier experiments are limited to a few thousand events in any specific channel. In addition, the photon is a fundamentally different probe than a π or K.

The current experimental situation in photoproduction is sparse at best and a unique opportunity now exists using high intensity polarized photon beams available at a $12\,GeV$ CEBAF to radically change this. With tagged photon intensities between 10^7 and 10^8 per second, it will be possible to generate data samples comparable or larger than all other meson production reactions. This will allow a full partial wave analysis, which in turn will allow us to identify both normal $q\bar{q}$ mesons, as well as non–$q\bar{q}$ states. The addition of linear polarization will both simplify the partial wave analysis, and improve our understanding of the production mechanisms.

Improving the situation in photoproduction is a primary goal of the proposed HALL D experiment at Jefferson Lab [halld99]. A cut-away view of the proposed HALL D detector is shown in Fig. 28. The detector is a nearly 4π hermetic device for both charged particles and photons. This will allow complete reconstruction of most final states, and when coupled with the linearly polarized photon beams, will allow for high statistics partial wave analyses of many different final states.

7.0.4 Current photoproduction data

Table 21 is a partial compilation of known photoproduction cross sections and the numbers of events from the existing experiments. The typical cross sections range from of order $0.1\,\mu$b up to of order $10\,\mu$b, with most measurements involving rather small numbers of events, typically on the order of a few thousand. These experiments

Reaction	E_γ *GeV*	σ (μb)	*Events*	*Ref.*
$\gamma p \to p\pi^+\pi^-$	9.3		3500	[ballam73]
$\gamma p \to p\pi^+\pi^-$	19.3		20908	[abe84]
$\gamma p \to p\pi^+\pi^-\pi^\circ$	2.8		2159	[ballam73]
$\gamma p \to p\pi^+\pi^-\pi^\circ$	4.7		1606	[ballam73]
$\gamma p \to p\pi^+\pi^-\pi^\circ$	9.3		1195	[ballam73]
$\gamma p \to p\pi^+\pi^-\pi^\circ$	4.7–5.8	$13.5 \pm 1.5\,\mu b$	3001	[eisenberg72]
$\gamma p \to p\pi^+\pi^-\pi^\circ$	6.8–8.2	$11.8 \pm 1.2\,\mu b$	7297	[eisenberg72]
$\gamma p \to n\pi^+\pi^+\pi^-$	4.7–5.8	$4.6 \pm 1.4\,\mu b$	1723	[eisenberg72]
$\gamma p \to n\pi^+\pi^+\pi^-$	6.8–8.2	$4.0 \pm 1.2\,\mu b$	4401	[eisenberg72]
$\gamma p \to n\pi^+\pi^+\pi^-$	16.5–20		3781	[condo93]
$\gamma p \to p\pi^+\pi^-\pi^\circ$	20–70		14236	[atkinson84]
$\gamma p \to p\pi^+\pi^-\pi^+\pi^-$	4–6	$4.0 \pm 0.5\,\mu b$	~ 330	[davier73]
$\gamma p \to p\pi^+\pi^-\pi^+\pi^-$	6–8	$4.8 \pm 0.5\,\mu b$	~ 470	[davier73]
$\gamma p \to p\pi^+\pi^-\pi^+\pi^-$	8–12	$4.5 \pm 0.6\,\mu b$	~ 470	[davier73]
$\gamma p \to p\pi^+\pi^-\pi^+\pi^-$	12–18	$4.4 \pm 0.6\,\mu b$	~ 380	[davier73]
$\gamma p \to p\pi^+\pi^-\pi^+\pi^-$	15–20		6468	[abe85]
$\gamma p \to p\pi^+\pi^-\pi^\circ\pi^\circ$	20–70		8100	[atkinson84a]
$\gamma p \to p\pi^+\pi^+\pi^-\pi^-\pi^\circ$	19.5		2553	[blackett97]
$\gamma p \to \Delta^{++}\pi^-\pi^+\pi^-$	4–6	$1.65 \pm 0.2\,\mu b$	~ 200	[davier73]
$\gamma p \to \Delta^{++}\pi^-\pi^+\pi^-$	6–8	$1.8 \pm 0.2\,\mu b$	~ 200	[davier73]
$\gamma p \to \Delta^{++}\pi^-\pi^+\pi^-$	8–12	$1.1 \pm 0.2\,\mu b$	~ 200	[davier73]
$\gamma p \to \Delta^{++}\pi^-\pi^+\pi^-$	12–18	$1.15 \pm 0.2\,\mu b$	~ 200	[davier73]
$\gamma p \to p\omega$	4.7–5.8	$2.3 \pm 0.4\,\mu b$	< 1600	[eisenberg72]
$\gamma p \to p\omega$	6.8–8.2	$2.0 \pm 0.3\,\mu b$	< 1200	[eisenberg72]
$\gamma p \to p\omega$	4.7	$3.0 \pm 0.3\,\mu b$	1354	[ballam73]
$\gamma p \to p\omega$	9.3	$1.9 \pm 0.3\,\mu b$	1377	[ballam73]
$\gamma p \to p\phi$	4.7	$0.41 \pm 0.09\,\mu b$	136	[ballam73]
$\gamma p \to p\phi$	9.3	$0.55 \pm 0.07\,\mu b$	224	[ballam73]
$\gamma p \to n a_2^+$	4.7–5.8	$1.7 \pm 0.9\,\mu b$		[eisenberg72]
$\gamma p \to n a_2^+$	6.8–8.2	$0.9 \pm 0.9\,\mu b$		[eisenberg72]
$\gamma p \to n a_2^+$	19.5	$0.29 \pm 0.06\,\mu b$	~ 100	[condo93]

Table 21: A sample of measured photoproduction cross sections from several references. Note the small numbers of events in any given channel.

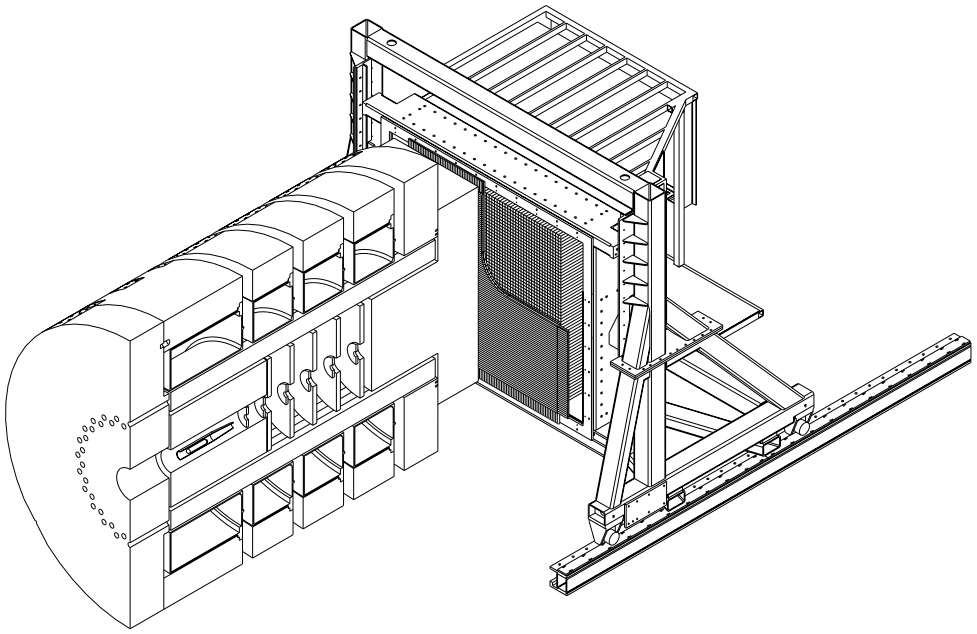

Figure 28: A cut-away view of the proposed HALL D detector.

were able to perform careful spin analyses, from which much was learned. However, the statistics were insufficient for a full partial wave analysis. This situation can be radically improved in photoproduction experiments at CEBAF, where a full partial wave analysis involving both production and many decay channels will be possible. Typically, these analyses divide the photoproduction data into bins of *invariant mass* and $\mid t \mid$. A reasonable grid might be 5 bins in $\mid t \mid$ between 0.0 and 1.0 $(GeV/c^2)^2$, and 0.01 GeV/c^2 wide bins in mass. Making the following conservative assumptions allow one to estimate a typical year's worth of data.

- The tagged photon flux is $\Phi = 10^7 s^{-1}$. The tagger sees a 3 GeV energy bite which tops out at 95% of the electron beam energy, E_e. (Hall B can currently tag five times this rate.)

- The total photoproduction cross section for a reaction $\gamma p \rightarrow NX$ is $\sigma = 1.0\,\mu$b. This is independent of the photon energy, and distributed over the m_x vs t plane using a t–dependent weight, $e^{-8|t|}$. It should be noted that the slope parameter of 8 $(GeV/c^2)^{-2}$ is at the high end of expected slopes, which range from 4 to 8 $(GeV/c^2)^{-2}$.

- The experiment runs for 300 days per year with 33% live time.

- The overall reconstruction efficiency is 10%

In Fig. 29 are shown the expected number of events collected under the above assumptions for E_e=6.0, 8.0, 10.0 and 12.0 GeV. Fig. 29(a) is a sum over all $\mid t \mid$ between 0 and 1.0 $(GeV/c^2)^2$ and shows on order of 100000 events per mass bin. Fig. 29(b)

through (f) show the events binned in $\mid t \mid$. Due to the $e^{-8|t|}$ dependence of the cross section, the number of events per t–bin falls off rapidly for the higher t bins. However, even in the highest t bin, there are still several hundred events per mass bin, which is quite sufficient to perform a full partial wave analysis.

To conclude, Fig. 30 shows a comparison between the current πp data for producing 3π final states compared to similar data for photoproduction, (note the factor of 1000 in the number of π events). One can see that there is a different shape to two spectra. Unfortunately, the photon data is so limited in statistics, that a full partial wave analysis is not possible. With the proposed HALL D experiment, we hope to completely change the landscape as far as photo production data goes, and plan to unravel the spectrum of gluonic excitations which is just starting to emerge from other experiments. The future of light–quark spectroscopy will likely be one of photon beams.

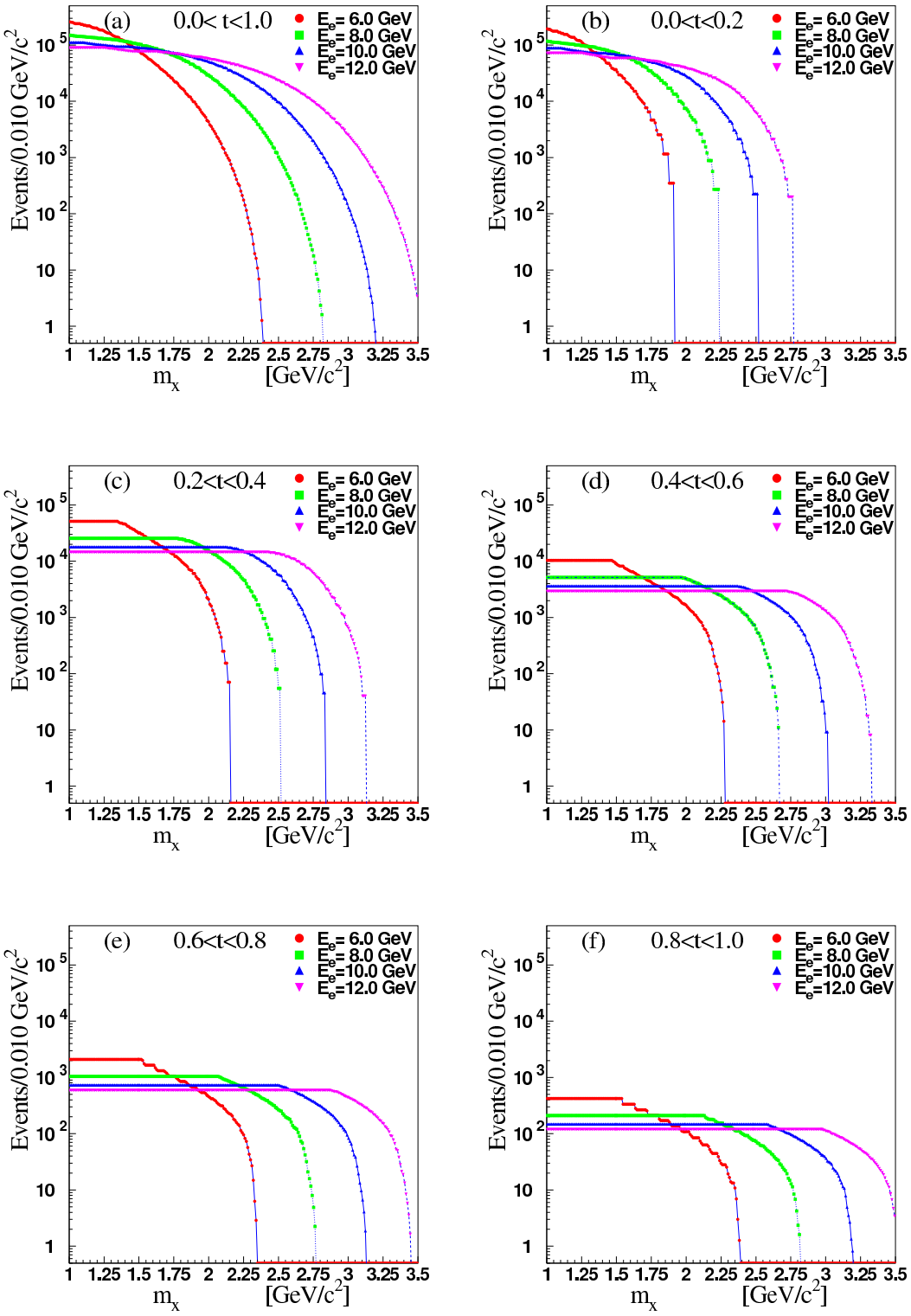

Figure 29: Expected numbers of events from the reaction $\gamma p \rightarrow Xp$ for 0.010 GeV wide bins in m_x.The data assume an energy independent total cross section of $\sigma = 1.00 \mu b$. The four curves are from top to bottom for E_e = 6 GeV, E_e=8 GeV, E_e=10 GeV and E_e=12 GeV.

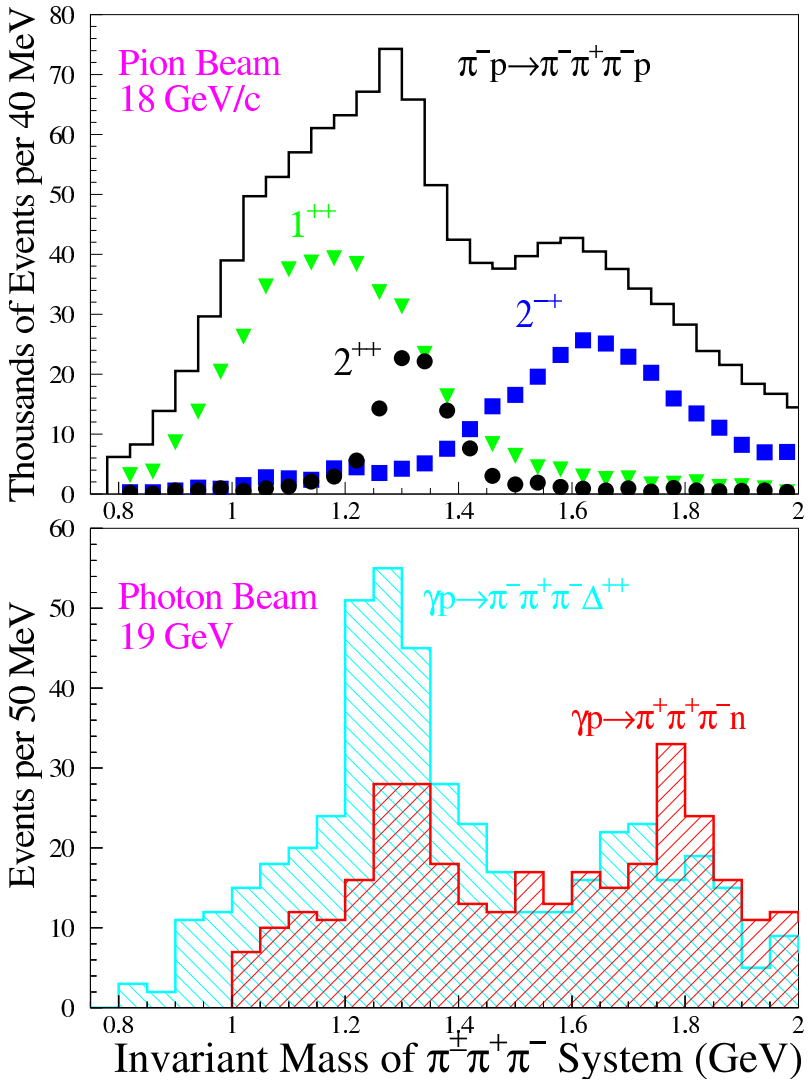

Figure 30: A comparison of pion peripheral production and photoproduction data.

References

[abe84] K. Abe *et al.*, *Phys. Rev. Lett.* ***53***, 751, (1984).

[abe85] K. Abe *et al.*, *Phys. Rev. D****32***, 2288, (1985).

[abele98] A. Abele, *et al.*, The Crystal Barrel Collaboration, **Exotic $\eta\pi$ state in $\bar{\mathrm{p}}$d annihilation at rest into $\pi^-\pi^\circ\eta$p**, *Phys. Lett. B****423***, 175, (1998).

[abele98] A. Abele, *et al.*, The Crystal Barrel Collaboration, **Evidence for a $\pi\eta$–P–wave in $\bar{p}p$–annihilation at rest into $\eta\pi^\circ\pi^\circ$**, *Phys. Lett. B****446***, 349, (1999).

[adams98] G. S. Adams, *et al.*, The E852 Collaboration, **Observation of a new $\mathbf{J^{PC} = 1^{-+}}$ exotic state in $\pi^-\mathrm{p} \to \pi^+\pi^-\pi^-\mathrm{p}$ at 18 GeV/c**, *Phys. Rev. Lett.* ***81***, 5670, (1998).

[afanasev98] A. Afanasev and P. R. Page, **Photoproduction and electroproduction of $J^{PC} = 1^{-+}$ exotics**, *Phys. Rev. D****57***, 6771, (1998).

[aker92] E. Aker, *et al.*, The Crystal Barrel Collaboration. **The Crystal Barrel Detector at LEAR**, *Nucl. Instrum. Methods A****321***, 69, (1992).

[amsler83] C. Amsler and J. C. Bizot, **Simulation of Angular Distributions and Correlations in The Decay of Particles with Spin**, *Comp. Phys. Comm.* ***30***, 21, (1983).

[amsler94a] C. Amsler, *et al.*, The Crystal Barrel Collaboration. **$\eta\eta'$ threshold enhancement in $\bar{p}p$ annihilation into $\pi^\circ\eta\eta'$ at rest**. *Phys. Lett. B****340***, 259, (1994).

[amsler95a] C. Amsler, *et al.*, The Crystal Barrel Collaboration. **A high statistics study of the $f_0(1500)$ decay into $\pi^\circ\pi^\circ$**. *Phys. Lett. B****342***, 433, (1995).

[amsler95b] C. Amsler, *et al.*, The Crystal Barrel Collaboration. **Coupled channel analysis of $\bar{p}p$ annihilation into $\pi^\circ\pi^\circ\pi^\circ$, $\pi^\circ\pi^\circ\eta$ and $\pi^\circ\eta\eta$**. *Phys. Lett. B****355***, 425, (1995).

[amsler95c] C. Amsler, *et al.*, The Crystal Barrel Collaboration. **A high statistics study of the $f_0(1500)$ decay into $\eta\eta$**. *Phys. Lett. B****358***, 389, (1995).

[amsler96a] C. Amsler, *et al.*, The Crystal Barrel Collaboration. **Observation of the $f_0(1500)$ decay into K_LK_L**. *Phys. Lett. B****385***, 425, (1996).

[amsler96] C. Amsler and F. E. Close, **Is the $\mathbf{f_0(1500)}$ a scalar glueball?**, *Phys. Rev. D****53***, 295, (1996).

[amsler98] Claude Amsler, **Proton-antiproton annihilation and meson spectroscopy with the Crystal Barrel**, *Rev. Mod. Phys.* ***70***, 1293, (1998).

[atkinson84] M. Atkinson *et al*, The Omega Collaboration. *Nucl. Phys.* ***B231***, 15, (1984).

[atkinson84a] M. Atkinson *et al*, The Omega Collaboration. *Nucl. Phys.* ***B243***, 1, (1984).

[bai96] J. Z. Bai, *et al.*, The BES Collaboration. **Structure Analysis of the $f_J(1710)$ in the Radiative Decay $J/\Psi \to \gamma K^+K^-$**, *Phys. Rev. Lett.* ***77***, 3959, (1997).

[bali93] G. S. Bali, *et al.*, The UKQCD Colaboration, **A comprehensive lattice study of SU(3) glueballs**, *Phys. Lett.* ***B309***, 378, (1993).

[bali98] G. Bali *et al.* (SESAM Collaboration). *Nucl. Phys. Proc. Suppl.*, **63**:209, 1998.

[ballam73] J. Ballam *et al.*, **Vector-meson production by polarized photons from 2.8, 4.7, and 9.3 GeV**, *Phys. Rev.* ***D7***, 3150, (1973).

[barberis95] D. Barberis, *et al.*, The WA102 Collaboration, **A further study of the centrally produced $\pi^+\pi^-$ and $\pi^+\pi^-\pi^+\pi^-$ channels in pp interactions at 300 and** 450 GeV/c, *Phys. Lett.* ***B353***, 589, (1995).

[barberis96] D. Barberis, *et al.*, The WA102 Collaboration, **Observation of vertex factorisation breaking in central pp interactions**, *Phys. Lett.* ***B388***, 853, (1996).

[barberis97a] D. Barberis, *et al.*, The WA102 Collaboration, **A kinematical selection of glueball candidates in central production**, *Phys. Lett.* ***B397***, 339, (1997).

[barberis97b] D. Barberis, *et al.*, The WA102 Collaboration, **A study of the centrally produced $\pi^+\pi^-\pi^+\pi^-$ channel in pp interactions at** 450 GeV/c, *Phys. Lett.* ***B413***, 217, (1997).

[barberis99a] D. Barberis, *et al.*, The WA102 Collaboration, **A partial wave analysis of centrally produced K^+K^- and K_SK_S systems in pp interactions at** 450 GeV/c **and new information on the spin of the $f_J(1710)$**, *Phys. Lett.* ***B453***, 305, (1999).

[barberis99b] D. Barberis, *et al.*, The WA102 Collaboration, **A partial wave analysis of centrally produced $\pi^+\pi^-$ system in pp interactions at** 450 GeV/c, *Phys. Lett.* ***B453***, 316, (1999).

[barberis99c] D. Barberis, *et al.*, The WA102 Collaboration, **A partial wave analysis of centrally produced $\pi^\circ\pi^\circ$ system in pp interactions at** 450 GeV/c, *Phys. Lett.* ***B453***, 325, (1999).

[barberis99d] D. Barberis, *et al.*, The WA102 Collaboration, **coupled channel analysis of the centrally produced K^+K^- and $\pi^+\pi^-$ system in pp interactions at** 450 GeV/c. Submitted to *Phys. Lett. B*, (1999), (`hep-ex/9907055`).

[barnes97] T. Barnes, F. E. Close, P. R. Page and E. S. Swanson, **Higher Quarkonia**, *Phys. Rev. D**55***, 4157, (1997).

[beladidze93] G. M. Beladidze, *et al.*, The VES Collaboration, **Study of $\pi^-N \to \eta\pi^-N$ and $\pi^-N \to \eta'\pi^-N$ reactions at 37 GeV/c**, *Phys. Lett. B**313***, 276, (1993).

[bernard97] C. Bernard *et al.*, *Phys. Rev. D***56**, 7039, (1997).

[bernard99] C. Bernard *et al.*, *Nucl. Phys. B(Proc. SUppl.)***73**, 264, (1999).

[blackett97] G. R. Blackett *et al.*, **The Photoproduction of the $b_1(1235)\pi$ System**, `hep-ex/9708032`.

[bugg95] D. Bugg, *et al.*, **Further amplitude analysis of $J/\Psi \to \gamma(\pi^+\pi^-\pi^+\pi^-)$**, *Phys. Lett. B**353***, 378, (1995).

[burakovsky98] L. Burakovsky and P. R. Page, **Scalar Glueball Mixing and Decay**, *Phys. Rev. D**59***, 014022, (1999).

[caso98] C. Caso, *et al.*, the Particle Data Group, *Eur. J. Phys. C**3***, 1, (1998).

[chanowitz84] M. Chanowitz, *Proceedings of the VI International Workshop on Photon–Photon Collisions*, Lake Tahoe, CA, Sept 10–13, World Scientific, 1985, R. L. Lander ed..

[chung71] S. U. Chung, CERN Report 71-8 (CERN, Geneva, 1971).

[chung96] S. U. Chung, J. Brose, R. Hackmann, E. Klempt, S. Spanier and C. Strassburger, **Partial wave analysis in K–matrix formalism**, *Ann. Phys. (Leipzig)* ***4***, 404, (1995).

[chung99] S. U. Chung, *et al.*, The E852 Collaboration,**Evidence for exotic $\mathbf{J^{PC} = 1^{-+}}$ meson production in the reaction $\pi^-p \to \eta\pi^-p$ at** 18 GeV/c, *Phys. Rev. D* ***60***, 092001, (1999).

[close79] F. E.Close, **An Introduction to Quarks and Partons**, (1979), Academic Press, Harcourt Brace Jovanovich.

[close88] F. E. Close, **Gluonic Hadrons** *Rep. Prog. Phys.* ***51***, (1988).

[close95] F. E. Close and P. R. Page, **Photoproduction of hybrid mesons from CEBAF to DESY HERA**, *Phys. Rev. D**52***, 1706, (1995).

[close97] F. E. Close, G. R. Farrar and Z. Li, **Determining the gluonic content of isoscalar mesons**, *Phys. Rev. D.**55***, 5749, (1997).

[close01] Frank E. Close and Andrew Kirk, **Scalar Glueball-$q\bar{q}$ Mixing above 1 GeV and implications for Lattice QCD**, *Eur. Phys. J. C* **21**, 531-543 (2001), hep-ph/0103173.

[condo91] G. T. Condo, *et al.*, **Photoproduction of an isovector $\rho\pi$ state at 1775 MeV**, *Phys. Rev. D* ***43***, 2787, (1991).

[condo93] G. T. Condo *et al.*, *Phys. Rev. D* ***48***,3045, (1993).

[cooper88] S. Cooper, **Meson Production in Two–Photon Collisions**, *Ann. Rev. Nucl. Part Phys.* ***38***, 705, (1988).

[davier73] M. Davier *et al.*, **The reaction $\gamma p \to \pi^+\pi^-\pi^+\pi^- p$ at high-energy and γ dissociation into 4π**, *Nucl. Phys. B* ***58***, 31, (1973).

[donnachie98] Alexander Donnachie and Philip R. Page, **Interpretation of experimental $\mathbf{J^{PC}}$ exotic signals**, *Phys. Rev. D* ***58***, 114012, (1998).

[dunwoodie97] W. Dunwoodie, **J/Ψ Radiative Decay to Two Pseudoscalar Mesons from Mark III** (1997), SLAC-PUB-7163.

[dzierba00] A. R. Dzierba, C. A. Meyer and E. S. Swanson, **The Search for QCD Exotics**, *American Scientist* **88**, 406, (2000).

[eisenberg72] Y. Eisenberg *et al.*, *Phys. Rev. D* ***5***, 15, (1972).

[flatte76] S. M. Flatté, *Phys. Lett B* ***63***, 224, (1976).

[genz83] H. Genz, *Phys. Rev. D* ***28***, 1094, (1983).

[godfrey99] Stephen Godfrey and Jim Napolitano, **Light Meson Spectroscopy**, submitted to *Rev. Mod. Phys.*, (1999), hep-ph/9811410.

[halld99] The Hall D Collaboration, **Photoproduction of Unusual Mesons, Design Report, Version2**, August 1999, http://www.phys.cmu.edu/halld/cdr/.

[herndon75] D. Herndon, P. Söding and R. J. Cashmore, *Phys. Rev. D* ***11***, 3165, (1975).

[isgur85] N. Isgur and J. Paton, **Flux–tube model for hadrons in QCD**, *Phys. Rev. D* ***31***, 2910, (1985).

[isgur85a] N. Isgur, R. Kokoski and J. Paton, **Gluonic Excitations of Mesons: Why they are missing and where to find them**, *Phys Rev Lett.* **54**, 869, (1985).

[jacobs59] M. Jacobs and G. C. Wick, *Ann. Phys.* ***7***, 404, (1959).

[juge99] K. J. Juge, J. Kuti and C. Morningstar, *Phys. Rev. Lett.* **82**, 4400, (1999).

[lacock97] P. Lacock *et al.*, *Phys. Lett. B*$\mathbf{401}$, 309, (1997).

[lacock99] P. Lacock and K. Schilling, *Nucl. Phys. B (Proc. Suppl.)*$\mathbf{73}$, 261, (1999).

[lee98] W. Lee and D. Weingarten, **Scalar Quarkonium Masses and Mixing with the Lightest Scalar Glueball**, (1998), (`hep-lat/9805029`)

[manke-99] T. Manke *et al.*, *Phys. Rev. Lett.*$\mathbf{82}$, 4396, (1999).

[morningstar99] C. Morningstar and M. Peardon, **The Glueball Spectrum from and Anisotropic Lattice**, *Phys. Rev. D****60***, 034509, (1999).

[morningstar01] C. Morningstar, **The study of exotic hadrons in lattice QCD.**

[nambu70] Y. Nambu, *Univ. of CHicago report No. 70-70*, (1970).

[nambu76] T. Nambu, **The Confinement of Quarks**, *Sci. Am.*$\mathbf{235}$, No.5, 48-70, (1976).

[page97] F. E. Close and P. R. Page, **Distinguishing hybrids from radial quarkonia**, *Phys. Rev. D****56***, 1584, (1997).

[page99] P. R. Page, E. S. Swanson and A. P. Szczepaniak, **Hybrid Meson Decay Penomenology**, *Phys. Rev. D*$\mathbf{59}$, 034016 (1999).

[pdg02] K. Hagiwara *et al.*, **Review of Particle Physics**, *Phys. Rev.D*$\mathbf{66}$, 010001, (2002).

[richman84] Jeffery D. Richman, **An Experimenter's Guide to the Helicity Formalism**, Caltech report CALT-68-1148, (1984).

[sexton95] J. Sexton, A. Vaccarino and D. Weingarten **Numerical Evidence for the Observation of a Scalar Glueball**, *Phys. Rev. Lett.* ***75***, 4563, (1995).

[thompson97] D. R. Thompson, *et al.* The E852 Collaboration, **Evidence for Exotic Meson Production in The Reaction $\pi^-\mathbf{p} \to \eta\pi^-\mathbf{p}$ at 18 GeV/c**, *Phys. Rev. Lett.* ***79***, 1630, (1997).

[weingarten97] Don Weingarten, **Scalar Quarkonium and the Scalar Glueball**, *Nucl. Phys. Proc. Suppl.* ***53***, 232, (1997).

[zemach64] Charles Zemach, **Three-Pion Decays of Unstable Particles**, *Phys. Rev.****140***, B1201, (1964).

[zhong02] Zhong-Hao Mei and Xiang-Qian Luo, **Exotoc mesons from quantum chromodynamics with improved gluon and quark actions on the anisotropic lattice**, (2002), (`hep-lat/0206012`).